Haploinsufficiency of the essential gene RpS12 causes defects in erythropoiesis and hematopoietic stem cell maintenance

Virginia Folgado-Marco* (1), Kristina Ames* (2,3), Jacky Chuen (1), Kira Gritsman (2,3) & Nicholas E. Baker (1)

(1) Department of Genetics, Albert Einstein College of Medicine

(2) Department of Medicine, Albert Einstein College of Medicine

(3) Department of Cell Biology, Albert Einstein College of Medicine

* These authors contributed equally

Corresponding authors:

Nicholas E. Baker: nicholas.baker@einsteinmed.org

Kira Gritsman: kira.gritsman@einsteinmed.org

Abstract

Ribosomal protein (Rp) gene haploinsufficiency can result in Diamond-Blackfan Anemia (DBA), characterized by defective erythropoiesis and skeletal defects. Some mouse Rp mutations recapitulate DBA phenotypes, although others lack erythropoietic or skeletal defects. We generated a conditional knockout mouse to partially delete *RpS12*, which results in homozygous embryonic lethality. *Rps12*$^{+/-}$ mice have growth and morphological defects, pancytopenia and impaired erythropoiesis. A striking reduction in hematopoietic stem cells (HSCs) and progenitors in the bone marrow (BM) was associated with decreased ability to repopulate the blood system after competitive and non-competitive BM transplantation. The mutants exhibited loss of HSC quiescence, which was associated with ERK and MTOR activation and increased global translation in HSC and progenitors. Thus, RpS12 has a very strong requirement in maintaining HSC quiescence and function, in addition to erythropoiesis that is affected in DBA patients.

Introduction

In the cell, protein synthesis is one of the most energetically expensive processes, and both the specificity and overall level of translation are tightly regulated. The ribosome is the macromolecular machine tasked with translating mRNAs into proteins and, as such, plays an essential role in the physiology of the cell. Ribosomes are evolutionarily conserved ribonucleoprotein complexes composed of ribosomal RNA (rRNA) and ribosomal proteins (Rp) (Yonath and Franceschi 1998; Wilson and Doudna Cate 2012). They catalyze protein synthesis in all cell types, providing a supply line of steady-state levels of necessary cellular proteins (Wilson and Doudna Cate 2012). The functional components of the ribosome are highly conserved, and in higher eukaryotes consist of a small subunit (40S) and a large subunit (60S). These ribosomal subunits contain a total

of 79 ribosomal proteins in eukaryotes, including 34 ribosomal proteins that are also conserved in prokaryotes (Petibon et al. 2020). In most cell types, ribosomal protein genes are among the most highly expressed genes (Geiger et al. 2012; Ji et al. 2019). Most ribosomal proteins are essential for ribosome biogenesis and function, which makes them essential for cell growth and proliferation (de la Cruz et al. 2015).

Given the importance of ribosomes, mutations in components of the ribosome or the ribosome biogenesis pathway in humans result in a group of diseases known as ribosomopathies. Despite the essential role of the ribosome in all cell types, this group of diseases is characterized by the presence of defects in specific tissues. Heterozygous loss of function mutations in Rp genes lead to Diamond-Blackfan Anemia (DBA), a congenital bone marrow failure syndrome characterized by macrocytic anemia, skeletal defects, and increased cancer risk. In DBA patients, mutations have been identified in 21 out of the 79 existing Rp genes, along with the GATA1 transcription factor (Ulirsch et al. 2018). Strikingly, in approximately 30-40% of DBA patient cases a mutation has not yet been identified. The fact that only a subset of all Rp genes have been found altered in DBA patients poses the question of whether mutations in any Rp gene can result in DBA and, if not, what would be the consequences for mutations in those Rp genes.

The generation and characterization of mice with mutations in Rp genes in recent years has begun to shed light on this question. Mutations in Rp genes of both the large and the small ribosomal subunits have been found to have similar phenotypes to those of DBA patients, such as impaired erythropoiesis, skeletal defects, and increased incidence of cancer, including some *Rp* not yet implicated in DBA (Oliver et al. 2004; McGowan et al. 2008; Jaako et al. 2011; Terzian et al. 2011; Morgado-Palacin et al. 2015;

Schneider et al. 2016). However, erythropoietic defects are not always reported for mutants in Rp genes, including some that are implicated in human DBA (Matsson et al. 2004; Watkins-Chow et al. 2013; Kazerounian et al. 2016). In addition, a variety of other defects are reported in particular genotypes, ranging from embryonic lethality to brain defects, pigmentation defects, and defects in other aspects of hematopoiesis (McGowan et al. 2008; Kondrashov et al. 2011; Terzian et al. 2011; Watkins-Chow et al. 2013; Morgado-Palacin et al. 2015).

The *RpS12* gene, which is not yet implicated in DBA, reportedly has special functions in *Drosophila* that differ from those of most Rp. Heterozygous loss of 66 out of the 79 *Drosophila Rp* genes result in a 'Minute' phenotype, named for its small adult sensory bristles and also characterized by delayed development (Marygold et al. 2007). Additionally, 'Minute' $Rp^{+/-}$ cells are eliminated by wild-type (WT) neighboring cells when they are found together in developing tissues, by a process known as cell competition (Morata and Ripoll 1975; Clavería and Torres 2016; Baker 2020). Remarkably, delayed development, reduced translation, cell competition and other aspects of the 'Minute' phenotype depend on the RpS12 protein, which seems to be required for haploinsufficient effects of other *Rp* genes, suggesting that RpS12 acts as a sensor or reporter of deficits in other Rp. Accordingly, increasing the copy number of *RpS12* enhances these 'Minute' phenotypes caused by mutations in other *Rp* genes, whereas reducing the *RpS12* gene copy number suppresses them (Kale et al. 2018; Boulan et al. 2019; Ji et al. 2019). Interestingly, *RpS12* is one of the few Rp genes whose null mutation does not present a 'Minute' phenotype in heterozygosis (Marygold et al. 2007; Kale et al. 2018). In mammals, it has been shown that RpS12 deletions are frequent in diffuse large B cell lymphoma

96 samples, and that RpS12 distribution in the ribosomes was altered under hypoxic
97 conditions in the human embryonic kidney cell line, HEK293, resulting in changes of their
98 translatome (Derenzini et al. 2019; Brumwell et al. 2020). Human RpS12 has also
99 emerged as a candidate regulator of Wnt secretion in cancer cells (Katanaev et al. 2020).
100 However, the phenotype of *RpS12* deletion in mammals has not been determined.

101 Protein synthesis regulation is important in stem cells. To maintain proper
102 homeostasis, hematopoietic stem cells (HSCs) sustain the balance between a quiescent
103 and an actively dividing state (Cabezas-Wallscheid et al. 2017). Quiescent HSCs require
104 low rates of protein synthesis, and even HSCs exiting quiescence still exhibit significantly
105 lower translation rates than in more differentiated progenitors. Both increases and
106 decreases in protein synthesis levels can impair HSC function (Signer et al. 2014; Hidalgo
107 San Jose et al. 2020).

108 The AKT/MTORC1 signaling pathway is one of the most well-known signaling
109 pathways that regulates translation, in part through the expression of ribosomal proteins
110 and translation factors (Fonseca et al. 2014). Hyperactivation of AKT signaling pathway
111 is deleterious for normal HSC function, and results in increased HSC cycling, with
112 depletion of the stem cell pool (Yilmaz et al. 2006; Kharas et al. 2010; Lee et al. 2010;
113 Magee et al. 2012). Activation of AKT by stem cell factor (SCF) and other growth factors
114 leads to the activation of MTOR, which results in the phosphorylation of the ribosomal
115 protein S6 kinase 1 (S6K1) and the protein initiation factor 4E binding protein1 (4EBP1)
116 (Gentilella et al. 2015). Phosphorylation of S6 by S6K1 at Serine 235/Ser236 is
117 associated with increased protein translation (Krieg et al. 1988; Roux and Topisirovic
118 2018). Additionally, phosphorylation of 4E-BP1 by MTOR at the Thr37 and Thr46 residues

primes it for dissociation of 4E-BP1 from eIF4E, also activating translation (Schalm et al. 2003). Furthermore, another important pathway regulating growth and translation, the MEK/ERK pathway, has been shown to phosphorylate S6 at Serine 235/Ser236 promoting the translation preinitiation complex in mammalian cells (Roux et al. 2007).

To further explore the specific functions of Rp genes, their potential involvement in DBA, and the regulation of translation, we determined the phenotype of RpS12 deletion in mice. We generated a conditional knock-out mouse, *RpS12*$^{flox/flox}$, which, when crossed to embryonically expressed Ella-Cre recombinase, allowed us to generate homozygous (*RpS12*$^{-/-}$) and heterozygous knock-out mice (*RpS12*$^{+/-}$). We report that, while homozygous loss of *RpS12* is lethal at early stages of embryogenesis, the *RpS12*$^{+/-}$ phenotype includes reduced body size, skeletal defects, and, in some cases, hydrocephalus and stroke. Similar to DBA patients, and some other previously published Rp mouse mutants, *RpS12*$^{+/-}$ mice present a block in erythroid maturation, lower red cell counts, and decreased spleen size. However, loss of RpS12 also leads to a striking reduction in the number of hematopoietic stem cells in the bone marrow, as well as significantly altered progenitor populations, leading to overall reduced bone marrow cellularity and a decreased ability of *RpS12*$^{+/-}$ BM cells to repopulate the blood system, uncovering an impairment in HSC and progenitor function. These phenotypes were associated with increased translation and loss of quiescence in HSCs.

Results

RpS12 haploinsufficiency results in a pleiotropic phenotype, including delayed growth and increased mortality

To test the role of the RpS12 protein in a mammal, we used CRISPR gene editing to generate a mouse line with *LoxP* sites flanking exons 2 and 3 of the endogenous *RpS12 locus* (*RpS12^{flox}*) (Supp Fig.1). Excision of these 2 exons generates an allele that cannot produce functional RpS12 protein, since exon 2 contains the ATG translation initiation codon. We chose not to eliminate the entire *RpS12* locus, to avoid deleting the small nucleolar RNA genes Snord100 and Snora33, which are located in introns 4 and 5, respectively (Supp Fig. 1). We crossed *RpS12$^{flox/flox}$* mice to a line that expresses the Cre recombinase embryonically (*EIIa-Cre*) to obtain RpS12 heterozygous knock-out (KO) mice (*RpS12$^{KO/+}$)* (Fig. 1A). Unlike heterozygous null flies, which don't have any observable phenotype (Marygold et al. 2007; Kale et al. 2018), *RpS12$^{KO/+}$* mice have reduced growth rates post-partum in comparison to their wild-type littermates (Fig. 1B, C). Additional phenotypes include kinked tails, mild hyperpigmentation of the footpads, and an increased risk of hydrocephalus (Fig. 1D, E, F). Although hydrocephalus has not been reported previously, some of these phenotypes have also been found in other ribosomal protein (Rp) mutant mouse models (Oliver et al. 2004; McGowan et al. 2008; Terzian et al. 2011). Furthermore, *RpS12$^{KO/+}$* mice have increased mortality, especially in early post-natal stages, most of which is associated with hydrocephalus or the inability to gain weight (Fig. 1G).

To investigate if the KO allele of *RpS12* is lethal in the homozygous state, and whether *RpS12$^{KO/+}$* animals have reduced growth during embryonic development, we crossed heterozygous *RpS12$^{KO/+}$* male and female mice and analyzed the resulting embryos at stage E13.5 (we could not assess frequencies in pups at birth because *RpS12$^{KO/+}$* females invariably died during labor). There were no *RpS12$^{KO/KO}$* specimens

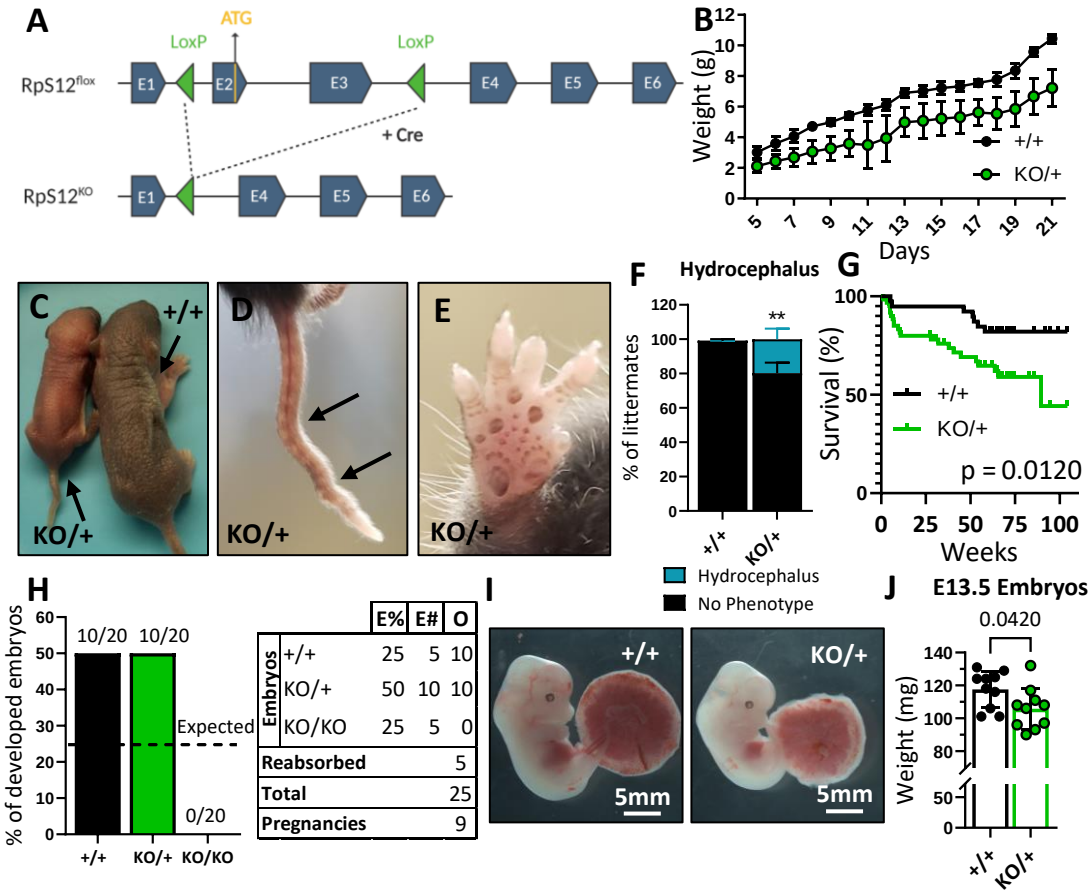

Figure 1. Loss of one copy of RpS12 results in delayed growth, morphologic defects, and reduced viability.

(A) Conditional *RpS12^{flox}* transgenic knock-in has two loxP sites flanking exons 2 and 3, that are removed by Cre recombinase activity to generate *RpS12^{KO}*. **(B)** Post-natal growth curve of *RpS12$^{KO/+}$* and *RpS12$^{+/+}$* littermates (+/+ n=8 and KO/+ n=11 pups). **(C)** Picture of 5-day-old *RpS12$^{KO/+}$* and *RpS12$^{+/+}$* littermates. **(D)** Representative picture of "kinked" tail in *RpS12$^{KO/+}$* mouse. **(E)** Representative picture of the anterior footpad hyperpigmentation in *RpS12$^{KO/+}$*. **(F)** Quantification of the percentage of mice presenting hydrocephalus per litter (n=27 litters, 2-way ANOVA p=0.0035). **(G)** Kaplan-Meier survival curves of *RpS12$^{KO/+}$* and RpS12$^{+/+}$ littermates starting at day 5 of age (+/+ n=39 and KO/+ n=60, log-rank Mantel-Cox test p=0.012). **(H)** Embryo genotype segregation from crosses between RpS12$^{KO/+}$ male and female. Graph represents percentage of developed embryos and the table shows the total numbers (E%=expected percentages, E#=expected numbers, O=observed numbers). **(I)** Representative pictures of E13.5 embryos with their placentas. **(J)** E13.5 embryo weights (n=10 on each genotype, unpaired t-test p=0.0420).

among the embryos obtained (Fig. 1H), which led us to conclude that this genotype must be lethal prior to stage E13.5. Furthermore, *RpS12*$^{KO/+}$ embryos are smaller in size compared to their wildtype counterparts (Fig. 1I, J). Therefore, these results indicate that *RpS12* is an essential gene, whose homozygous loss leads to early embryonic lethality, and heterozygous loss causes reduced growth starting in embryogenesis, in addition to other defects recognized post-partum.

Heterozygous loss of RpS12 results in erythropoiesis defects that worsen with age

We sought to understand if, similar to other Rp mutant mouse models, RpS12 heterozygous mutants have anemia or defective erythropoiesis. Analysis of peripheral blood counts showed that “young” (6-8 weeks old) *RpS12*$^{KO/+}$ mice had lower number of white blood cells (WBC), red blood cells (RBC), and platelets, a condition known as pancytopenia (Fig. 2A). We also observed a high mean corpuscular volume (MCV), which is reminiscent of the macrocytic anemia seen in DBA patients.

To analyze erythropoiesis in *RpS12*$^{KO/+}$ mice, we used flow cytometry with the lineage markers Ter119 and CD71 on bone marrow and spleen cells (Fig. 2B). These populations represent different maturation stages of the red blood cell production process, which we refer to as RI (CD71^{+}, Ter119^{-}, proerythroblasts), RII (CD71^{+}Ter119^{+}, basophilic erythroblasts), RIII (CD71^{mid}, Ter119^{+}, late basophilic and polychromatophilic erythroblasts), and RIV (CD71^{-}Ter119^{+}, orthochromatic erythroblasts) (Socolovsky et al. 2001). Bone marrow samples from young *RpS12*$^{KO/+}$ mice showed a defective transition between the RII and RIII stage cells, while the erythropoiesis in spleen populations was unchanged (Fig. 2C, D). This impairment in erythropoiesis worsened with age, as

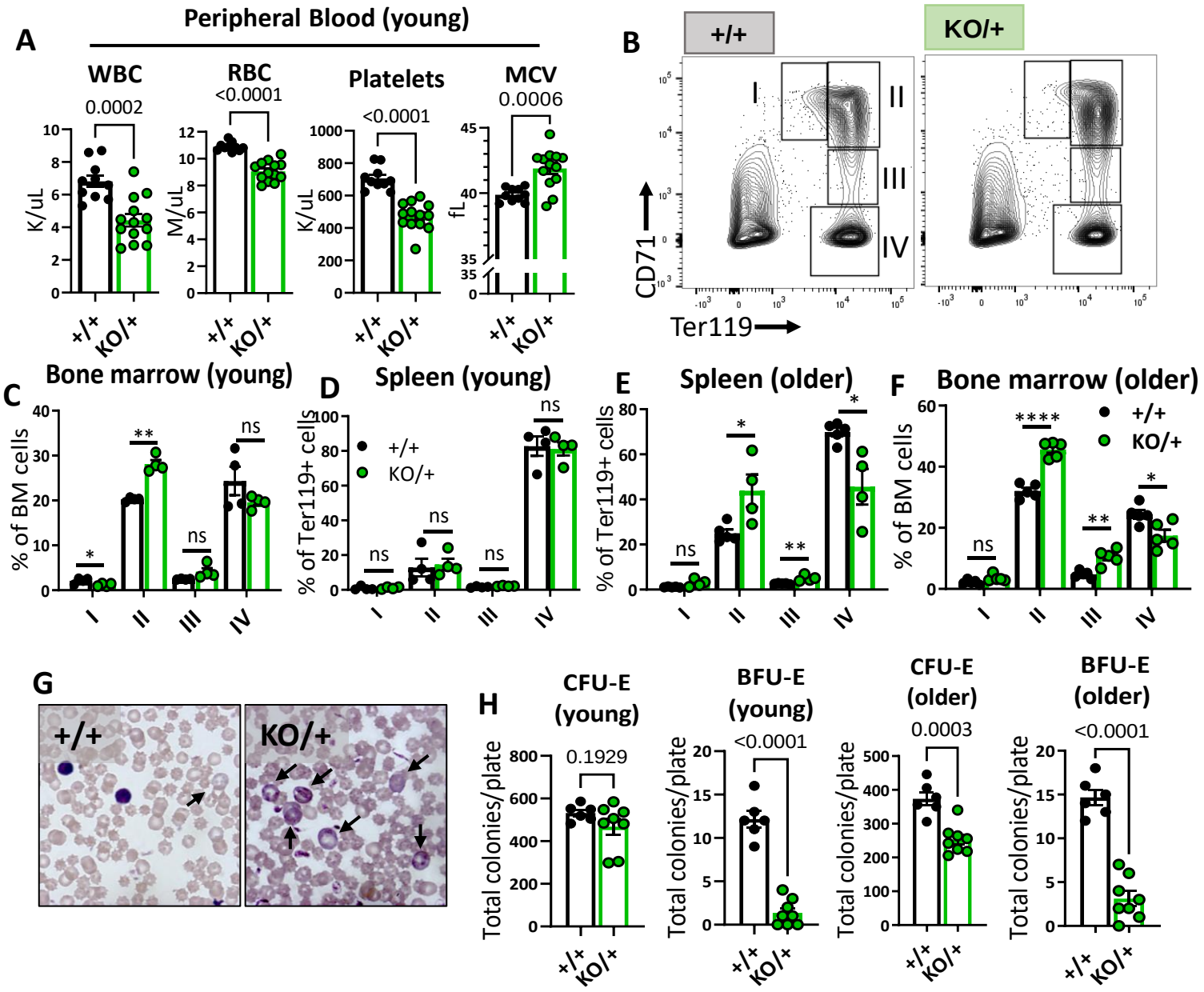

Figure 2. Haploinsufficiency of *RpS12* results in erythropoiesis defects that worsen with age.
(A) Quantification of peripheral blood counts from young (6-8 weeks) littermates (+/+ n=10 and KO/+ n=13) (WBC=white blood cells, RBC=red blood cell, MCV=mean corpuscular volume). **(B)** Representative flow cytometry gating of bone marrow cells from 6-8-weeks-old mice of erythropoietic populations using Ter119 and CD71 markers. **(C, D, E, F)** Frequencies of erythroid progenitors in bone marrow and spleen of young (6-7 weeks old, +/+ n=4 and KO/+ n=4) and older (6-7 months old, +/+ n=5 and KO/+ n=5) mice. **(G)** Representative images of stained peripheral blood smears indicating the presence of reticulocytes (arrows). **(H)** Total number of CFU-E and BFU-E colonies per plate ($5x10^5$ BM cells plated) in methylcellulose media supplemented with EPO (M3434) from young mice (6-7 weeks old, +/+ n=4 and KO/+ n=4, each biological sample had two replicates) and older mice (6-7 months old, +/+ n=4 and KO/+ n=4, each biological sample had two replicates).
Statistical analysis: quantifications represent mean +/-SEM, when only two groups were being compared, unpaired t-test was performed, and for multiple comparison one-way ANOVA analysis was used. *p < 0.05, **p < 0.01 , ***p < 0.001, ****p < 0.0001

188 samples from “older” (6-7 month-old) *RpS12*$^{KO/+}$ mice had a higher accumulation of RII
189 and RIII stage cells, while RIV population numbers were decreased in both spleen and
190 bone marrow samples at this age (Fig. 2E, F). In agreement with defective erythropoiesis,
191 peripheral blood samples showed a visibly elevated percentage of reticulocytes in Wright-
192 Giemsa stained blood smears (Fig. 2G). To assess erythropoietic progenitor function, we
193 performed colony-forming unit (CFU) assays in methylcellulose media optimized for the
194 differentiation of erythroid progenitors. Consistent with the observed impairment of
195 erythropoiesis, *RpS12*$^{KO/+}$ bone marrow cells generated fewer BFU-E colonies, indicating
196 reduced erythroid progenitor function (Fig. 2H). Altogether, these results show that RpS12
197 is required for erythroid differentiation, and demonstrate a role for Rps12 in
198 erythropoiesis, similar to what has been observed in mouse models of DBA genes like
199 *RpL11* or *RpS19* (Jaako et al. 2011; Morgado-Palacin et al. 2015).
200
201 **RpS12$^{KO/+}$ mice have a striking reduction in hematopoietic progenitor populations,**
202 **resulting in chronic pancytopenia**
203 We were intrigued by the fact that *RpS12*$^{KO/+}$ mice have pancytopenia (Fig. 2A),
204 since this is not a common feature of DBA patients. Due to the general decrease of
205 peripheral blood cell numbers in *RpS12*$^{KO/+}$ mice, we hypothesized that hematopoietic
206 stem and progenitor cells (HSPCs) might be affected. Using flow cytometry analysis, we
207 assessed the stem cell and progenitor populations in the bone marrow using previously
208 defined markers (Pietras et al. 2015) (Fig. 3A). Indeed, compared to the controls,
209 *RpS12*$^{KO/+}$ revealed a striking reduction in the numbers of long-term HSCs (LT-HSCs:
210 Flk2^{-}CD48^{-}CD150^{+} Lineage^{-}Sca1^{+}c-kit^{+} (LSK)) and short-term HSCs (ST-HSCs: Flk2^{-}

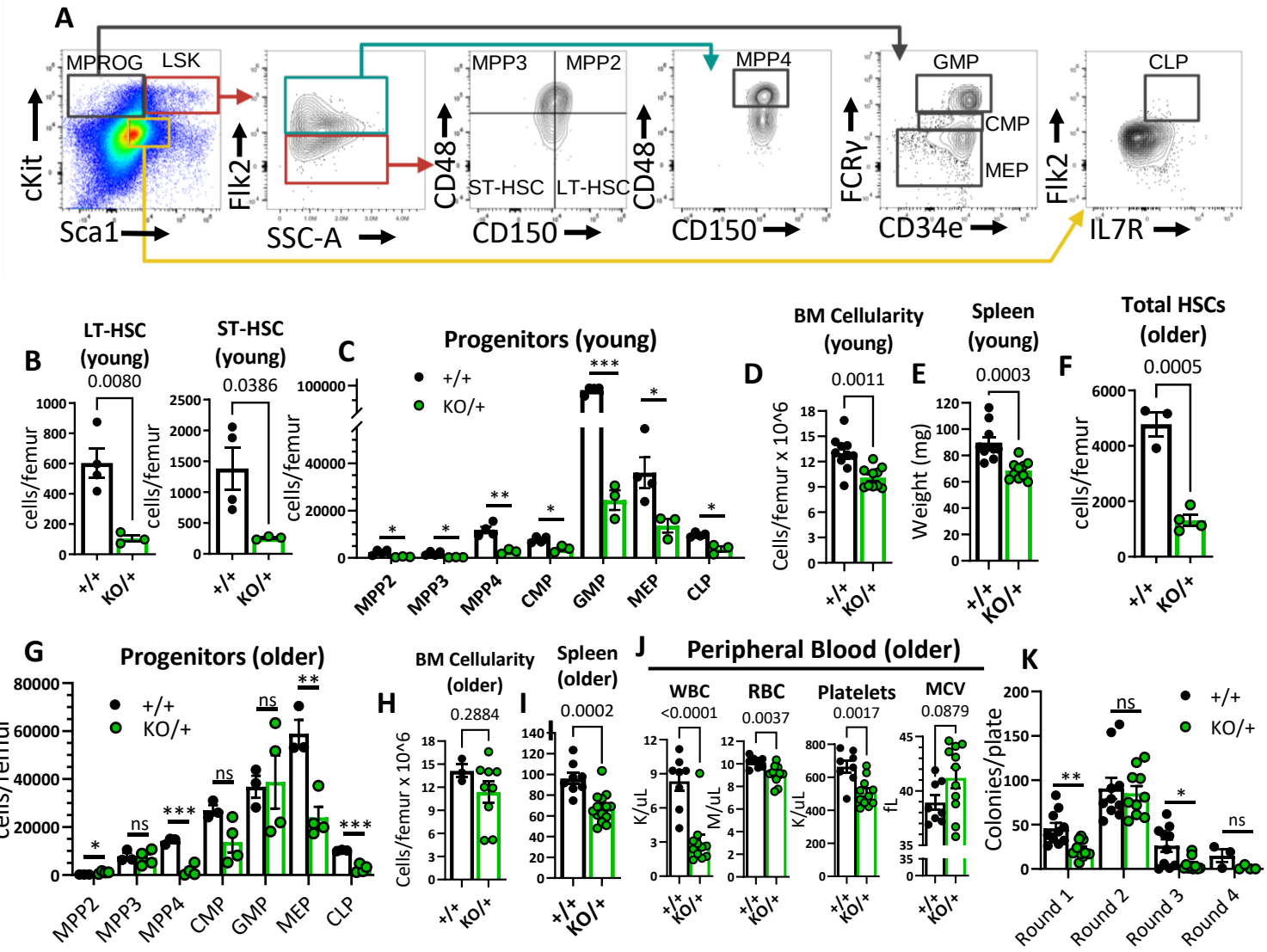

Figure 3. Reduced HSCs and other hematopoietic progenitor numbers in RpS12$^{KO/+}$ mice.

(A) Representative gating strategy used to identify bone marrow populations of LSKs: long-term HSC (LT- HSC), short-term HSC (ST-HSC), multi-potent progenitors (MPP2, MPP3, MPP4) and myeloid progenitors (MPROG): common myeloid progenitor (CMP), granulocyte-monocyte progenitor (GMP), megakaryocyte-erythrocyte (MEP) and common lymphoid progenitor (CLP). **(B)** Total LT-HSCs and ST-HSCs per femur of young mice (6-8 weeks old littermates, +/+ n=4 and KO/+ n=3). **(C)** Total number of cells per femur of indicated hematopoietic progenitor populations in young mice (6-8 weeks old littermates, +/+ n=4 and KO/+ n=3). **(D)** Bone marrow cellularity represented as cells per femur x10^6 from young mice (6-7 weeks old littermates, +/+ n=10 and KO/+ n=10). **(E)** Spleen weights of young (6-7 weeks old, +/+ n=10 and KO/+ n=10) mice. **(F)** Total HSCs per femur of older mice (6–7-month-old, +/+ n=3 and KO/+ n=4). **(G)** Total number of cells per femur of indicated hematopoietic progenitor populations in older mice (6–7-month-old, +/+ n=3 and KO+ n=4). **(H)** Bone marrow cellularity represented as cells per femur x10^6 from older mice (older: 6-7 months old, +/+ n=3 and KO/+ n=9). **(I)** Spleen weights of older (6-7 months old, +/+ n=8 and KO/+ n=14) mice. **(J)** Quantification of peripheral blood counts from older mice (6-7 months old, +/+ n=8 and KO/+ n=11). **(K)** Total number of colonies per plate (1x10^4 BM cells from 6-7-month-old mice plated in round 1 and 1x10^4 cells plated from previous plate on each re-plating round) on each round of re-plating in complete methylcellulose media (+/+ n=5 and KO/+ n=5, 2 replicates per biological sample).

Statistical analysis: quantifications represent mean +/-SEM, unpaired t-tests were performed to established significance among populations between genotypes *p < 0.05, **p < 0.01 , ***p < 0.001, ****p < 0.0001

CD48$^-$CD150$^-$ LSK) (Fig. 3B). In addition, in *RpS12*$^{KO/+}$ bone marrow, the numbers of all hematopoietic progenitor populations were significantly reduced (Fig. 3C). Accordingly, compared to the WT littermates, young (6-8-week-old) *RpS12*$^{KO/+}$ mice had lower bone marrow cellularity and decreased spleen weights (Fig.3D, E). Additionally, older (6-7-month-old) *RpS12*$^{KO/+}$ mice also had lower HSC numbers (Fig. 3F). Interestingly, we observed a partial recovery of some of the HSPC populations with age, such as multi-potent progenitors (MPP) 2 and 3, and the granulocyte-macrophage progenitors (GMP), as well as normalized overall BM cellularity, but not of spleen size (Fig. 3G, H, I). This, however, did not lead to improved blood counts (Fig. 3J), indicating that HSPC function was not significantly improved with age. Lastly, since RpS12 deletion resulted in decreased HSC and progenitor numbers, we assessed the self-renewal capacity of *RpS12*$^{KO/+}$ bone marrow cells. Plating assays in complete methylcellulose media showed a decreased clonogenic activity of *RpS12*$^{KO/+}$ bone marrow cells, as evidenced by the lower number of total colonies observed in the first round of plating (Fig. 3K). Additionally, *RpS12*$^{KO/+}$ cells have reduced serial replating capacity, suggesting decreased self-renewal capacity (Fig. 3K). Together, these results suggest that RpS12 plays an essential role in HSC function, including self-renewal and differentiation.

Heterozygous loss of RpS12 impairs ability of HSCs to reconstitute peripheral blood.

We assessed self-renewal and differentiation properties of *RpS12*$^{KO/+}$ bone marrow cells (CD45.2+) *in vivo* by transplanting bone marrow into lethally irradiated B6.SJL mice (CD45.1+) (Fig. 4A). Interestingly, compared to the *RpS12*$^{Flox/Flox}$ *or*

234 *RpS12*$^{Flox/+}$ controls, *RpS12*$^{KO/+}$ bone marrow recipients had decreased survival, with 5
235 out of 20 transplanted mice dying within the first 8 weeks in the *RpS12*$^{KO/+}$ group vs 0 out
236 of 20 dying in the control group (Fig. 4B). Whereas 100% of the control recipients were
237 able to reconstitute the bone marrow in the long term (up to 20 weeks), only 55% of the
238 *RpS12*$^{KO/+}$ recipients did so (Fig. 4C). Furthermore, longitudinal analysis of donor
239 chimerism in the peripheral blood revealed that compared to the controls, surviving
240 *RpS12*$^{KO/+}$ transplant recipients had significantly decreased donor chimerism
241 (%CD45.2+) in the B and T cell lineages, and a trend toward decreased chimerism in the
242 myeloid lineage (Fig. 4D-G). Together, this data suggests that bone marrow cells that
243 lack RpS12 are deficient in hematopoietic repopulating capacity after lethal irradiation.
244 To assess *RpS12*$^{KO/+}$ bone marrow cell repopulation capacity under more stringent
245 conditions, we performed competitive transplantation of control (*RpS12*$^{Flox/+}$) or *RpS12*$^{KO/+}$
246 bone marrow (CD45.2^{+}) mixed with competitor WT bone marrow from B6.SJL mice
247 (CD45.1^{+}) in a 1:1 ratio into lethally irradiated B6.SJL (CD45.1^{+}) recipient mice. Post-
248 transplantation we monitored donor chimerism in the peripheral blood over time and
249 analyzed the bone marrow chimerism at 20 weeks post-transplantation (Fig. 4H).
250 Compared to the controls, *RpS12*$^{KO/+}$ transplant recipients showed a striking decrease in
251 the percentage of donor-derived bone marrow cells and of HSCs (Fig. 4 I, J),
252 accompanied by significant and persistent reduction in peripheral blood total donor
253 chimerism in both myeloid and lymphoid lineages (Fig. 4K-N). Together, these data
254 suggest that RpS12 haploinsufficiency leads to perturbed HSC self-renewal, resulting in
255 ineffective hematopoiesis.
256

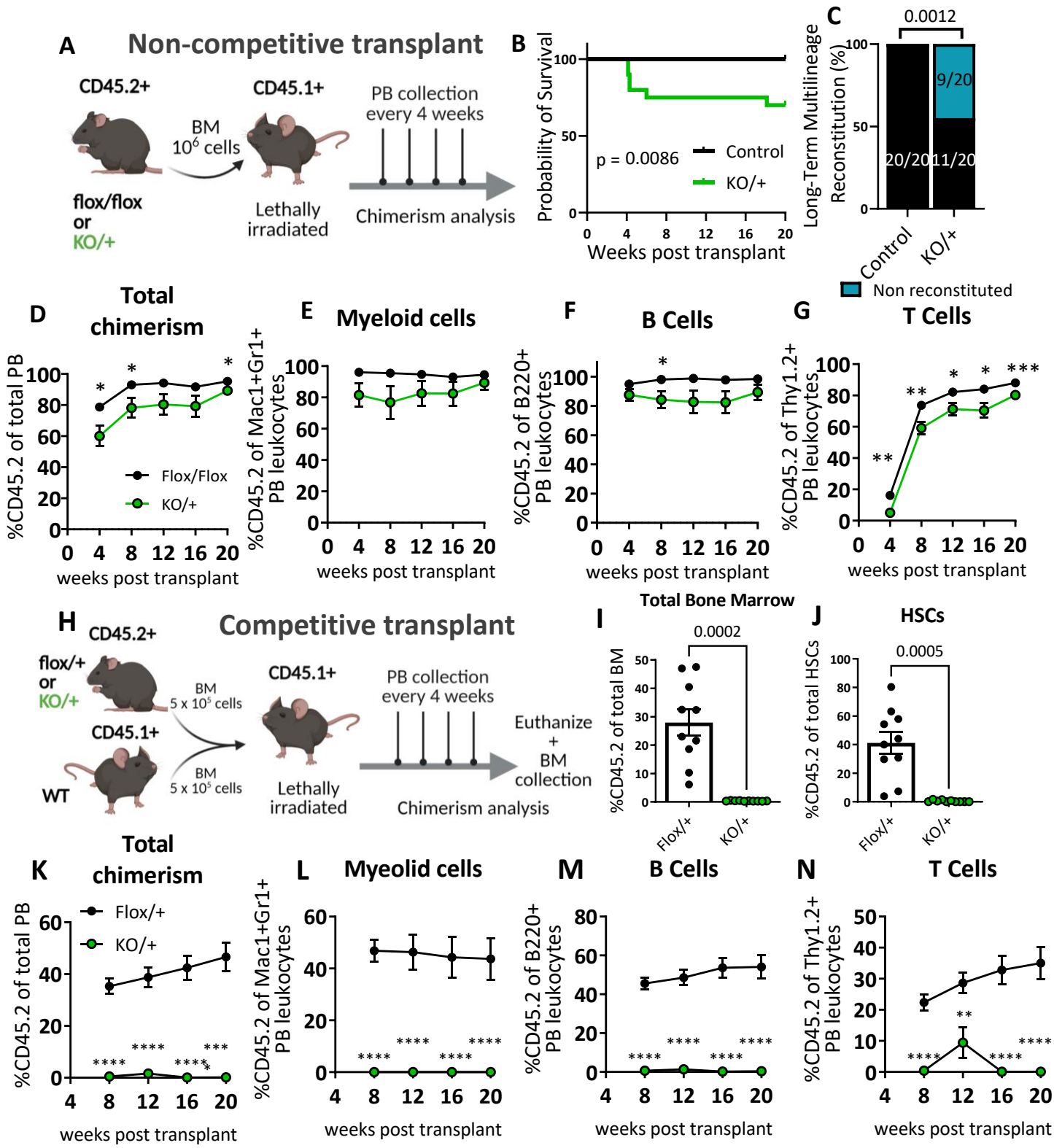

The embryonic hematopoietic system is largely unaffected in *RpS12$^{KO/+}$* animals

The striking reduction of hematopoietic progenitor numbers in *RpS12$^{KO/+}$* adult bone marrow prompted us to investigate if this phenotype could be a consequence of defective HSC production in the fetal liver during embryogenesis. We analyzed fetal liver hematopoietic populations of E13.5 *RpS12$^{+/+}$* and *RpS12$^{KO/+}$* embryos because it has been shown that HSC numbers increase, and differentiation begins, between days 12 and 16 of embryogenesis in this organ (Sugiyama et al. 2011). First, we looked at the gross morphology and cellularity of the liver, neither of which were significantly different between the genotypes (Fig. 5A, B). Next, we assessed different stages of erythropoiesis using Ter119 and CD71 markers as previously described in fetal liver (Magee and Signer 2021). Most of the cells in population V were lost during staining, and therefore we did not include them in our analysis. Compared to the control embryos, *RpS12$^{KO/+}$* embryos showed no apparent impairment in erythropoiesis in the fetal liver (Fig. 5C, D). Finally, we analyzed the distribution of HSPCs in E13.5 embryos. Overall, we did not observe any significant changes in the frequencies of LT-HSCs (CD48$^-$CD150$^+$ LSK), ST-HSCs (CD48$^-$ CD150$^-$ LSK), MPP (CD48$^+$ LSK), CMP, GMP or MEP populations (Fig. 5E-H). These results show that partial loss of RpS12 does not affect embryonic hematopoiesis by E13.5. Therefore, the later HSPC deficiency is not a consequence of a defect in embryonic specification.

RpS12$^{KO/+}$ HSCs and some hematopoietic progenitors show higher translation, cycling and apoptosis

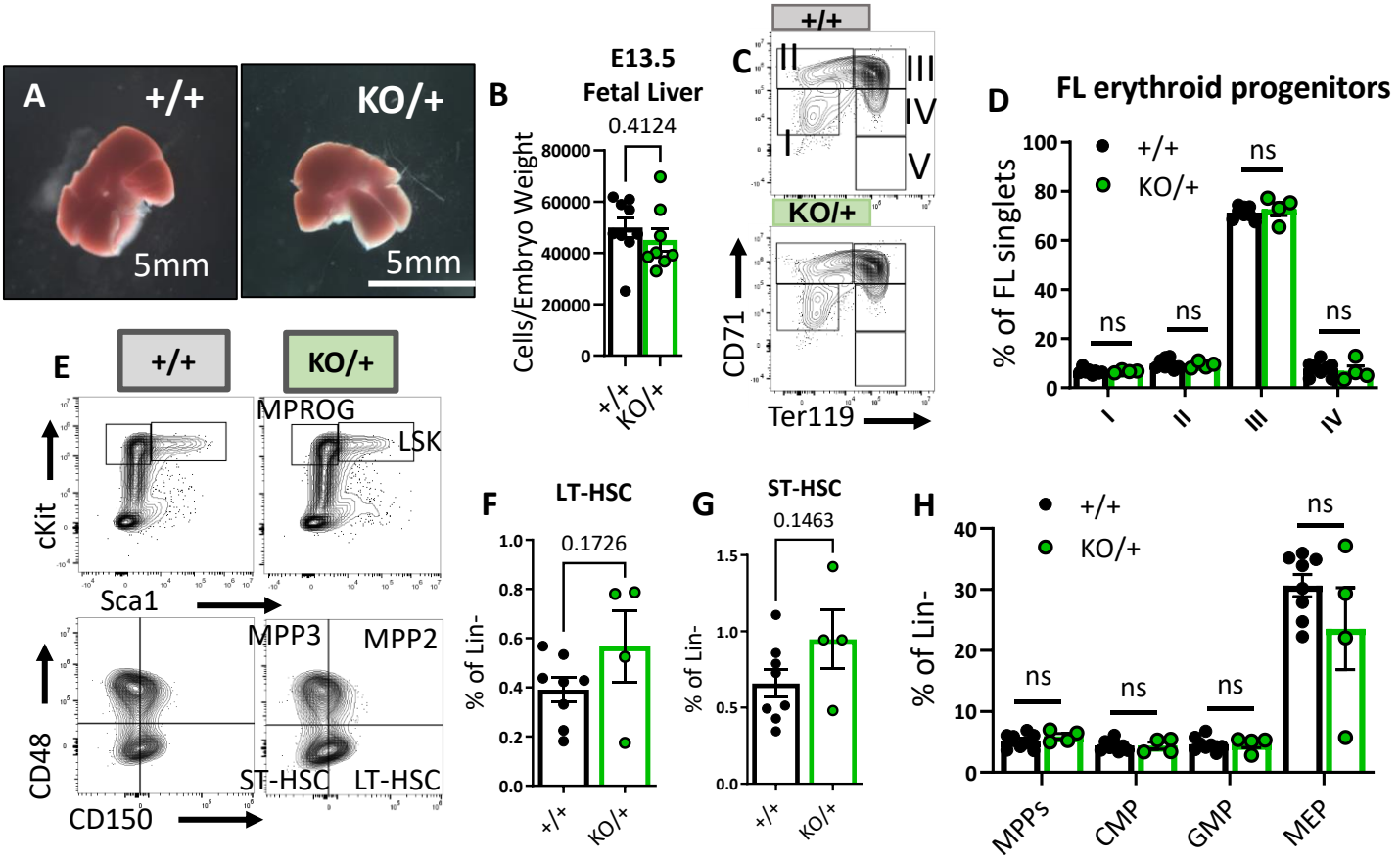

Figure 5. Embryonic hematopoietic system is largely unaffected in *RpS12$^{KO/+}$* animals.
(A) Representative images of RpS12$^{+/-}$ and littermate E13.5 fetal livers. **(B)** Quantification of total number of cells per liver, normalized to embryo weight (+/+ n=9 and KO/+ n=8). **(C)** Representative flow cytometry gating of erythropoietic populations using Ter119 and CD71 markers of fetal liver samples from E13.5 embryos. (E) Representative flow cytometry gating of Lin- (top) and LSK (bottom) populations in E13.5 fetal livers. **(F,G,H)** LT-HSCs, ST-HSCs and indicated progenitor populations represented as percentages of the Lin- population in E13.5 fetal livers. **(D,F,G,H)** Biological samples are +/+ n=8 and KO/+ n=4.
Statistical analysis: quantifications represent mean +/-SEM, unpaired t-tests were performed to established significance among populations between genotypes *p < 0.05, **p < 0.01 , ***p < 0.001, ****p < 0.0001

There are several important factors that maintain the HSC pool, including quiescence, low translation levels, and cell survival. We therefore analyzed the distribution of HSPCs among the cell cycle stages defined by the DNA content (Hoechst) and the levels of Ki67 (Fig. 6A). We observed a lower proportion of *RpS12*$^{KO/+}$ HSCs in the G0 stage of the cell cycle, and a significantly increased proportion in the actively cycling phases G1 and S/G2/M (Fig. 6B). Similar results were observed in MPP2/3 (LSK, Flk2^{-}, CD48^{+}), MPP4, and myeloid (MPROG) and common lymphoid progenitors (CLP) (Fig. 6B). These results show that compared to the control, *RpS12*$^{KO/+}$ HSCs are significantly less quiescent, with a higher proportion of HSCs and progenitors actively cycling.

Cell cycle activation generally requires translation, but previous studies have reported a generalized decrease in global translation in some Rp mutants, including in HSPC, despite a decrease in HSC quiescence (Oliver et al. 2004; Signer et al. 2014; Schneider et al. 2016). To test the global translation levels of each HSPC population in RpS12 heterozygous mice using flow cytometry, we performed an *in vitro* assay on freshly isolated HSCs and progenitors using the puromycin analog o-propargyl puromycin (OPP) as previously described (Signer et al. 2014). Unexpectedly, compared to the *RpS12*$^{+/+}$ controls, *RpS12*$^{KO/+}$ HSCs and multipotent progenitor cell populations all showed increased levels of global translation (Fig. 6C, D). The difference was especially remarkable in HSCs. Interestingly, compared to the controls, *RpS12*$^{KO/+}$ myeloid progenitors did not exhibit differences in OPP intensity, and among different myeloid progenitor populations, only the megakaryocyte-erythrocyte progenitors (MEP) had a significant increase in OPP incorporation (Fig. 6E). Thus, these data suggest that a

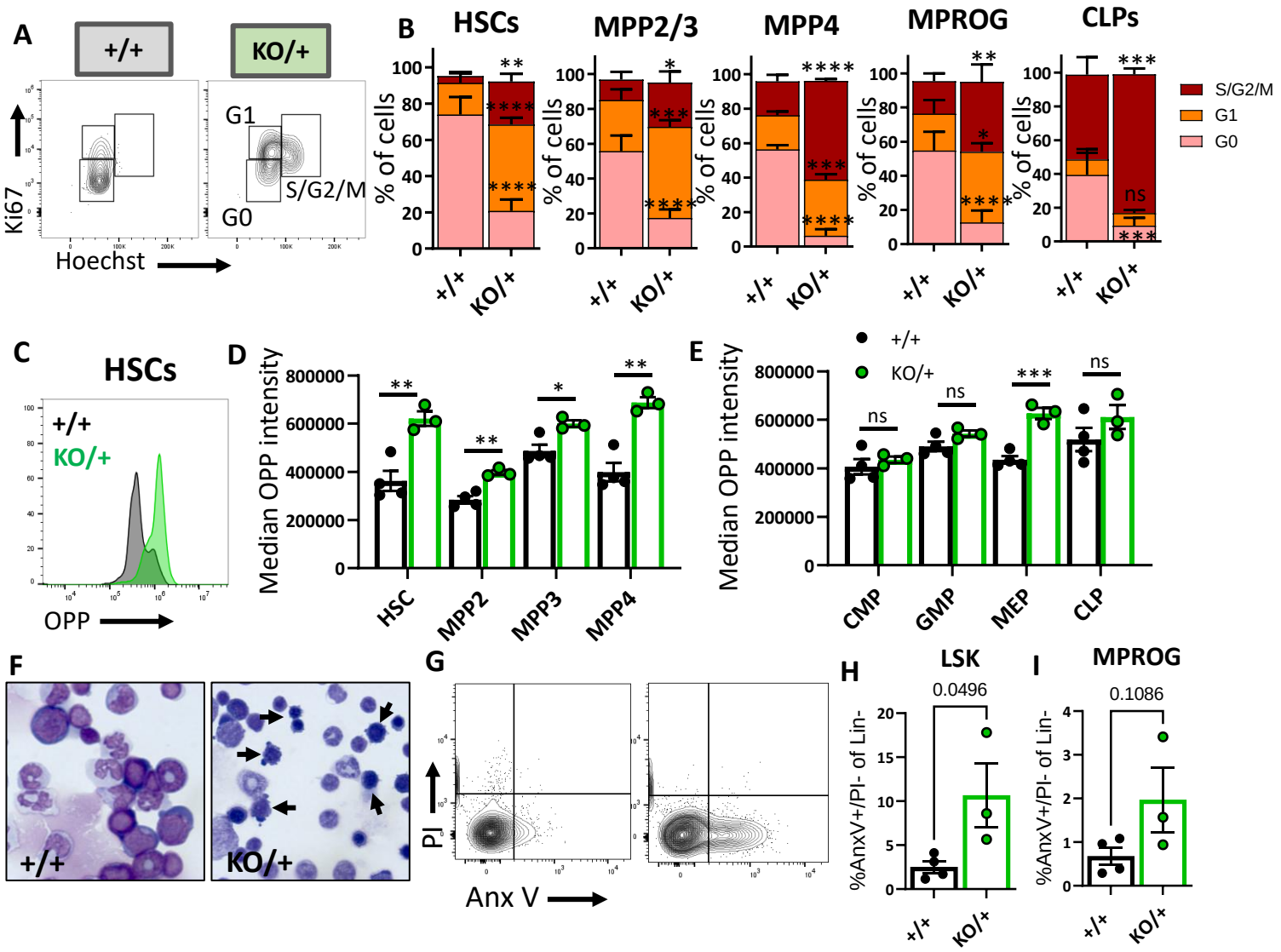

Figure 6. HSCs and other hematopoietic progenitors have altered cycling, global translation levels and apoptosis in *RpS12*$^{KO/+}$ bone marrow.

(A) Representative flow cytometry gating of HSCs (Flk2^{-}CD48^{-}LSK) cell cycle stages (G0, G1, S/G2/M) distribution determined by DNA (Hoechst) and Ki67 levels. **(B)** Cell cycle stages distribution in HSCs and in indicated progenitor populations. Asterisks correspond to p values assessing significant differences in each cell cycle stage between *RpS12*$^{KO/+}$ and *RpS12*$^{+/+}$ mice (6-8-weeks-old littermates, +/+ n=4 and KO/+ n=3). **(C)** Representative flow cytometry histogram showing OPP intensity in *RpS12*$^{KO/+}$ (green) and *RpS12*$^{+/+}$ (grey) HSCs. **(D, E)** Median OPP intensity of the indicated bone marrow populations (6-8-weeks-old littermates, +/+ n=4 and KO/+ n=3). This analysis was repeated in 6-7-month-old mice with similar results. **(F)** Representative images of bone marrow cytospins showing high number of apoptotic cells (arrows) in *RpS12*$^{KO/+}$ samples. **(G)** Representative flow cytometry gating of LIN- population showing apoptotic populations as determined by AnexinV and PI staining. **(H, I)** Percentage of apoptotic (AnnexinV+) cells in LSK (Lin^{-}cKit^{+}Sca1^{+}) and Myeloid progenitor (MPROG; Lin^{-}cKit^{+}Sca1^{-}) populations (6-8-weeks-old littermates, +/+ n=4 and KO/+ n=3).
Statistical analysis: quantifications represent mean+/-SEM, two-way ANOVA (B-F) and unpaired t-tests were performed to established significance among populations between genotypes *p < 0.05, **p < 0.01 , ***p < 0.001, ****p < 0.0001

decrease in Rps12 leads to an abnormal increase in global protein translation in immature bone marrow populations, including HSCs.

Cell death can deplete the HSC pool, and can result from chronic HSC activation. We asked whether this reduction of HSCs in *RpS12*$^{KO/+}$ animals is due to an increase in apoptosis. Interestingly, compared to controls, *RpS12*$^{KO/+}$ animals have an increased number of apoptotic cells in bone marrow cytospins (Fig. 6F). To quantify the level of apoptosis in the immunophenotypic populations of the bone marrow cells, we used the flow cytometry markers PI and Annexin V together with population-specific cell surface markers (Fig. 6G). Our flow analysis confirmed a significant increase in apoptosis in Lineage^{-}Sca1^{+}c-Kit^{+} (LSK) cells, a population that contains HSCs and MPPs, but not in more mature myeloid progenitors (Fig. 6H, I).

RpS12$^{KO/+}$ HSPCs have overactivated MEK/ERK and AKT/TOR signaling pathways

Because *RpS12*$^{KO/+}$ mutants have increased translation, we assessed the activity of the AKT/MTOR pathway, since it is known to regulate translation. Since the AKT/MTOR pathway is activated by stem cell factor (SCF), we determined the level of the AKT/MTOR pathway activation in the presence and absence of SCF, by assessing the phosphorylation levels of phospho-AKT (Ser 473) and the MTOR downstream effectors phospho-S6 (Ser235/236) and phospho-4E-BP1 (Thr37/46). Our results show that, in the more immature LSK population, which is enriched for HSCs and MPPs, the levels of p-AKT, p-S6 and p-4E-BP1 were significantly elevated in *RpS12*$^{KO/+}$ animals compared to wild-type littermates, not only upon stem cell factor (SCF) stimulation, but even at the non-stimulated baseline. Indeed, the *RpS12*$^{KO/+}$ genotype alone was a more potent

activator than SCF (Fig. 7A-C). Interestingly, this was not the case for the more mature myeloid progenitor cells, where the levels of p-AKT, p-S6 and p-4E-BP1 are comparable to the controls in both non-stimulated and SCF-stimulated conditions, and these cells also exhibited more normal translation rates (Fig. 7D-F). Since phosphorylation of S6 and 4EBP1 leads to increased translation, this data corroborates the increase in translation observed in the *RpS12*$^{KO/+}$ LSK population (Fig. 6D). Interestingly, more mature MPROG do not have increased translation (Fig. 6E) and do not have increased activation of the AKT/MTOR pathway (Fig. 7D-F). Together, these data suggest that activation of translation and the increase in AKT/MTOR signaling in *RpS12*$^{KO/+}$ mutant cells are specific to HSCs and MPPs.

Additionally, compared to wild-type controls, *RpS12*$^{KO/+}$ mutant animals also have increased phospho-ERK1 (Thr202/Tyr204) in the LSK and MPROG populations under SCF stimulated and non-stimulated conditions (Fig. 7G, H). Another regulator of translation is the eukaryotic initiation factor 2α (eIF2α), which is required for CAP-dependent translation initiation. Cells respond to several stress conditions by phosphorylating eIF2α, reducing global translation and upregulating stress-response genes (Wek et al. 2006; Sigurdsson and Miharada 2018). In skeletal muscle stem cells, eIF2α phosphorylation promotes quiescence and stem cell maintenance (Zismanov et al. 2016). Interestingly, compared to the control cells, *RpS12*$^{KO/+}$ cKit+ bone marrow progenitor cells show decreased levels of p-eIF2α (Fig.7I), which also correlates with increased translation.

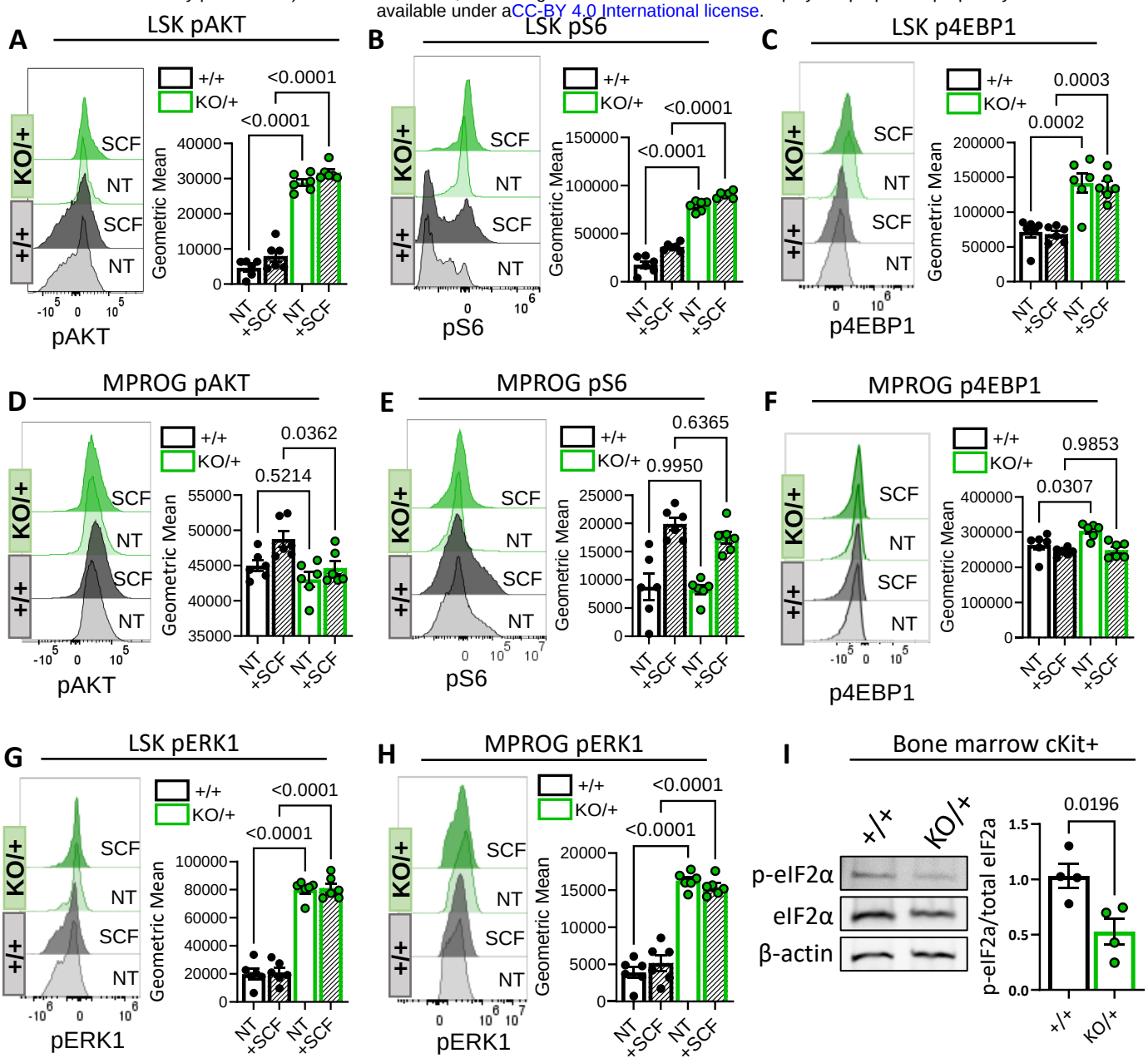

Figure 7. Decreased Rps12 levels leads to the excessive activation of the AKT/MTOR and ERK signaling pathways.

(A-H) Representative phospho-flow cytometry histograms and quantification of the normalized geometric mean fluorescent intensity of pAKT (Ser 473) **(A,D)**, pS6 (Ser235/236) **(B,E)**, p4EBP1 (Thr37/46) **(C,F)** and pERK1(Thr202/Tyr204) **(D,H)** signal in the LSK **(A,B,C,G)** and MPROG **(D,E,F,H)** bone marrow cell populations. Baseline signal was determined in the none treated (NT) serum starved cells, stimulation was done with the stem cell factor (SCF) *ex vivo* for 5 minutes. Immunophenotypic populations were defined as follows: LSK: Lin$^-$cKit$^+$Sca1$^+$, MPROG: Lin$^-$cKit$^+$Sca1$^-$. **(I)** Representative images of western blot analysis and quantification of phospho-eIF2α normalized to the total eIF2α protein in cKit-enriched BM samples (6-8-weeks-old littermates, +/+ n=4 and KO/+ n=4) **(A-H)** 7-weeks-old littermates, +/+ n=6 and KO/+ n=6 biological samples were used.

Statistical analysis: quantifications represent mean+/-SEM, one-way ANOVA Tukey's multiple comparison's test were performed to established significance among samples between genotypes

Discussion

We generated an RpS12 knock-out mouse and describe the homozygous and heterozygous mutant phenotypes. Homozygous loss of *RpS12* was lethal during early embryogenesis. Similar to other *Rp* mutant mice, *RpS12* heterozygous mutants have reduced body size, skeletal defects, and anemia, and we showed that RpS12 is required for erythroid differentiation. Some of the mice also exhibited hydrocephalus. Heterozygous mice were viable with several visible phenotypes and blood cell defects. In many respects, *RpS12* mutant phenotypes resemble those of mice mutant for other *Rp* genes, including defective erythropoiesis, suggesting that *RpS12* could be a candidate gene for DBA.

Most strikingly, we report that RpS12 is also crucial for normal hematopoietic stem cell self-renewal and differentiation, with defective engraftment and long-term repopulation of $Rps12^{KO/+}$ bone marrow in transplantation experiments. This seems specific to adult HSCs, as no hematopoietic defect was observed in the fetal livers of $RpS12^{KO/+}$ embryos. Although we have not determined whether the transition from the fetal liver to the bone marrow occurs normally, such a defect would only be expected to delay bone marrow engraftment, and does not seem sufficient to explain the chronically defective HSC function and striking loss of HSC quiescence that we observe in $RpS12^{KO/+}$ adult mice.

The loss of bone marrow HSC quiescence was associated with chronic activation of Akt/mTor and Erk, increased translation, and HSC apoptosis. Chronic activation of the AKT/MTOR pathway has been shown to result in increased HSC cycling, apoptosis, and

370 decreased self-renewal (Chen et al. 2008; Kharas et al. 2010), which could explain the
371 HSPC exhaustion phenotype and increased HSPC apoptosis in *RpS12*$^{KO/+}$ mice. Fetal
372 liver HSCs, which were unaffected in *RpS12*$^{KO/+}$, normally have a higher proliferative
373 activity and higher translation rates than adult HSCs (Magee and Signer 2021), which
374 may be why they are less sensitive to heterozygous deletion of RpS12.

375 The increase in HSPC-specific, global translation upon heterozygous deletion of
376 *RpS12* is the opposite of what has been reported in *RpL24*$^{Bst/+}$ and *RpS14*$^{+/-}$ HSPCs
377 (Signer et al. 2014; Schneider et al. 2016), although there are other *Rp* genotypes where
378 HSC cycling is increased (Terzian et al. 2011; Schneider et al. 2016). However, it is
379 consistent with the increased translation that has been reported in mice with deletion of
380 *Pten* in HSCs, which leads to activation of the AKT/MTOR pathway (Signer et al. 2014).
381 Importantly, detailed studies of RpS12 depletion from ribosomes in yeast clearly
382 demonstrate a strong reduction in translation as a result (Martin-Villanueva et al. 2020).
383 Unless RpS12 has a different function in mice, or in HSPCs, this raises the possibility that
384 enhanced translation in *RpS12*$^{KO/+}$ cells might be due, not to enhanced translation by
385 ribosomes lacking RpS12, but to increased activity of the remaining intact ribosomes that
386 contain RpS12. Such an increase would in fact be expected as a result of the striking
387 activation of the AKT/MTOR and ERK pathways. *RpS12*$^{KO/+}$ c-Kit+ hematopoietic
388 progenitors also have lower phosphorylated eIF2α, which would also predict higher
389 translation levels.

390 It remains to be determined how *RpS12* haploinsufficiency leads to activation of
391 the AKT/MTOR and ERK signaling pathways, which has not been reported in other *Rp*

mutants. It is interesting that a regulatory role has been suggested for RpS12 in *Drosophila*, where multiple properties of *Rp* mutant cells, including translation, depend on RpS12-dependent activation of a transcriptional stress response mediated by the *Drosophila* transcription factor Xrp1, although the molecular mechanism is not yet known (Kale et al. 2018; Boulan et al. 2019; Ji et al. 2019). It is possible that mouse RpS12, either through an effect on specific translation or otherwise, plays a particular role in regulating HSC quiescence, through the direct or indirect activation of the AKT/MTOR and ERK pathways. However, it is also possible that HSC activation occurs indirectly, as a consequence of HSC apoptosis. In addition, we cannot exclude the possibility that RpS12 deletion in the bone marrow niche could lead to a loss of HSC quiescence through a non-autonomous mechanism. Specific RpS12 functions that have been suggested in mammalian cells and cancers could now be explored using this conditional knock-out model with tissue specific Cre-drivers (Derenzini et al. 2019; Brumwell et al. 2020; Katanaev et al. 2020).

The fact that *RpS12*$^{KO/+}$ mice exhibit fully-penetrant pancytopenia with a severe bone marrow failure phenotype, in addition to the erythropoiesis defect, raises the possibility that *RpS12* might not have been found mutated in DBA patients due to a more severe human phenotype that is not classified as DBA. Perhaps only a hypomorphic *RpS12* genotype could be associated with DBA. It is also the case, however, that caution is required extrapolating from mouse phenotypes to human. Nevertheless, our study raises the possibility that Rps12 could in fact be a candidate gene not only for DBA, but for a broader group of bone marrow failure disorders. One of the reasons that genetic alterations in RpS12 have not yet been reported in DBA or other bone marrow failure

disorders could be that RpS12 is not included in the most common targeted next generation sequencing (NGS) panels used in the diagnosis of these disorders, some of which report molecular diagnostic rates of only 44-59% (Ghemlas et al. 2015; Muramatsu et al. 2017; Galvez et al. 2021). We suggest that in the future RpS12 should be included in expanded NGS panels for bone marrow failure disorders, or should be sequenced in the patients in whom there are no molecular findings in the standard NGS panels.

Methods

Generation of RpS12^{flox} knock-in mice

A pair of guide-RNAs (gRNAs) targeting intron 1 and intron 3 of *RpS12* gene respectively were designed by an online tool (http://crispr.mit.edu/) and generated by in vitro transcription. Cas9 mRNA was purchased from SBI. An *RpS12* conditional knockout homology-directed repair (HDR) plasmid containing 2kb homologous arms at each side and exon 2 and 3 flanked by loxP sites (Supp. Fig. 1) was generated by SLiCE cloning. Super ovulated female C57BL/6J mice (3–4 weeks old) were mated to C57BL/6J males, and fertilized embryos were collected from oviducts. The gRNAs, Cas9 mRNA and conditional knockout HDR plasmid were microinjected into the cytoplasm of fertilized eggs. The injected zygotes were transferred into pseudo pregnant CD1 females and the resulting pups were genotyped. Out of 20 pups, 2 mice were identified as *RpS12*$^{flox/+}$, which were then crossed to obtain *RpS12*$^{flox/flox}$ (*Rps12*^{em1Nbakr} MGI:6388411). The corresponding DNA sequences can be found in Supplementary table 1.

Mice

All animals were housed at the Animal Housing and Studies Facility at Albert Einstein College of Medicine (AECOM) under pathogen-free conditions and experiments were performed following protocols approved by the Institutional Animal Care and Use Committee (IACUC) (Protocol #20181206). C57BL/6J and EIIa-Cre (FVB/N-Tg(EIIa-cre)C5379Lmgd/J) mice were obtained from Jackson. B6.SJL-Ptprca/BoyAiTac (CD45.1) mice from Taconic were used for transplantation experiments. To generate *RpS12*$^{KO/+}$ mice, we crossed *RpS12*$^{flox/flox}$ to EIIa-Cre mice and used primers flanking the floxed region to identify progeny where recombination had occurred. Unless indicated, these mice were kept as heterozygous by crossing them with C57BL/6J and the presence of the EIIa-Cre locus was crossed out. In each case, the genotypes were confirmed by PCR using genomic DNA extracted from tails using DNeasy kit from Qiagen (#69504). Peripheral blood samples were collected via facial vein bleeding under isoflurane anesthesia, and blood counts obtained using the Genesis analyzer (Oxford Science). To generate growth curves, 5-day-old pups were genotyped and numbered by cutting toes. Pups' weight was measured daily from day 5 to day 21 of age.

Preparation of the single cell suspension

Bone marrow single cell suspension was prepared from freshly harvested femurs, tibiae, ilia, and vertebrae by gentle crushing of the bones in phosphate buffered saline containing 2% fetal bovine serum (PBS/2% FBS) followed by filtration through a 40-µm strainer. Spleen cells were obtained from freshly harvested spleens. Single cell suspension was prepared by dissociating spleens using the flat end of a plunger against in 40-µm strainers

and washed with PBS/2% FBS. Fetal liver single cell suspension was prepared from freshly harvested E13.5 fetal livers by passing through a 200-µl pipet tip and filtered through a 40-µm strainer in PBS/2% FBS. Cells were subjected to RBC lysis (Qiagen) according to the manufacturers protocol and used for the further steps described below. To calculate absolute number of cells per femur one femur per mouse was flushed, RBC lysed and cells counted to obtain total number of cells per femur.

Flow cytometry on live cells

Bone marrow: Single cell bone marrow suspensions were stained with a cocktail of biotin-conjugated lineage antibodies for 30min at 4°C, washed with PBS/2% FBS, stained with fluorochrome-conjugated antibody cocktails for 30min at 4°C, washed with PBS/2% FBS, resuspended in PBS/2% FBS, filtered through a 40-µm strainer, and subjected to Flow analysis. For the antibody panels, refer to Supplementary Tables 2 and 3.

Peripheral blood: samples were subjected to RBC lysis, blocked with CD16/CD32 10min at 4°C followed by staining with fluorochrome-conjugated antibodies, washed with PBS/2% FBS, resuspended in PBS/2% FBS, filtered through a 40-µm strainer and subjected to Flow analysis. For the antibody panels, refer to Supplementary Table 2 and 3.

Erythropoiesis analysis: Obtained single cell suspension of spleen cells (without RBC lysis) was blocked with CD16/CD32 for 10 min at 4°C and stained with fluorochrome-conjugated antibodies for 30 min at 4°C (Supplementary Table 3). E13.5 fetal livers single cell suspension was blocked with CD16/CD32 10min at 4°C and stained with

erythropoiesis or progenitor panels as described above. All blocking and staining steps were performed in PBS/2% FBS.

Apoptosis analysis: Single cell suspension samples were stained with the lineage-cocktail and fluorochrome-conjugated antibody cocktails as described above. After completion surface antibody staining, samples were incubated with FITC-conjugated Annexin V (BD-560931) and Propidium Iodide (BD-556463) following the manufacturer's instructions.

All flow cytometry was performed with BD FACS LSRII or Cytek Aurora and data analysis was done with FlowJo Software (v9, v10).

Flow cytometry on fixed cells

Cell cycle: Fresh single cell suspension of the RBC lysed bone marrow cells was stained with lineage antibodies followed by staining with fluorochrome-conjugated antibodies against surface markers, as described above. Immediately after staining cells were fixed and permeabilized using Cytofix/Cytoperm™ Fixation/Permeabilization Solution Kit (BD biosciences, BDB554714) according to the manufacturer's instructions. Followed fixation, cells were incubated overnight at 4°C with FITC-conjugated Ki67 antibody in Perm/Wash buffer. DNA was stained with 25µl/ml Hoechst in Perm/Wash buffer before flow cytometry analysis. Flow cytometry was performed with BD FACS LSRII or Cytek Aurora and data analysis was done with FlowJo Software (v9, v10).

Global translation *in vitro*: protocol was based on a previously described assay (Signer et al. 2014). Single cell bone marrow RBC lysed cell suspension was obtained as described. Cells were resuspended in DMEM (Corning 10-013-CV) media supplemented

with 50 µM β-mercaptoethanol (Sigma) and 20 µM OPP (Thermo Scientific C10456). Cells were incubated for 45 minutes at 37°C and then washed with Ca^{2+} and Mg^{2+} free PBS. The samples were stained with biotin-labeled antibodies, followed by staining with fluorochrome-conjugated antibody cocktails, fixed and permeabilized using Cytofix/Cytoperm™ as described above. After permeabilization with Perm/Wash buffer, cells were resuspended in Click-iT® Plus Reaction Cocktail (Thermo Scientific C10456) containing azide conjugated to Alexa Fluor 488 for 30 minutes at room temperature, washed once with Click-iT® Reaction Rinse Buffer and resuspended in Perm/Wash buffer. Flow cytometry was performed with Cytek Aurora and data analysis was done with FlowJo Software (v9, v10).

Phospho-flow cytometry: Bone marrow cells were starved for 1 hour in IMDM 2% FBS at 37°C, stained with lineage antibodies, followed by staining with fluorochrome-conjugated antibodies against surface markers, as described above. Post staining cells stimulated with 100ng/ml mSCF (Peprotech #250-03) in 2% PBS-FBS for 5 min at 37°C. Stained and stimulated cells were fixed and permeabilized with Cytofix/Cytoperm as described above and stained with phospho-S6 (Ser235/236) - Alexa 488 (Cell Signaling Technology, 4803S) (1:100) and phospho-AKT (Ser473) - Alexa647 (Cell Signaling Technology, 2337S), phospho-4E-BP1 (Thr37/46) -Alexa Fluor647 -(Cell Signaling Technology, 5123S) of pERK1(T202/Y204) - Alexa 488 (Cell Signaling 4374) at 1:20 dilutions. Cells were washed with Perm/Wash buffer to remove residual and unbound antibody, and resuspended in fresh Perm/Wash buffer, followed by flow cytometry analysis on the Cytek Aurora. Analysis of all flow cytometry data was performed using FlowJo software (v9, v10).

528

529 **Methylcellulose cultures and serial re-plating**

530 Single cell bone marrow suspensions (post RBC lysis) or single cell fetal liver cell
531 suspensions (without RBC lysis) were resuspended in RPMI media supplemented with
532 10%FBS and 1% penicillin/streptomycin. Cells were manually counted on a
533 hemocytometer using Trypan blue and plated in methylcellulose media (M3434 or M3334,
534 Stem Cell Technologies) at a density of $5x10^5$ live cells/ml (in M3434) or 10^4 live cells/ml
535 (in M3334) in 35mm cell culture plates. Samples were incubated at 37°C in 6.5% CO_2 at
536 constant humidity. Colonies were scored and evaluated 7-10 days after plating. To
537 replate, cells were washed from the plates with RMPI media, counted, and re-plated in
538 fresh M3334 methylcellulose at a density of 10^4 live cells/dish in 35mm plates. This
539 process was repeated until cell exhaustion in one of the experimental groups.

540

541 **Bone marrow transplantation**

542 6-8-week-old B6.SJL (CD45.1) recipient mice were lethally irradiated with a single dose
543 of 950 Gy using a Cesium-137 gamma-ray irradiator (Mark I irradiator Model 68) at least
544 3 hours before transplantation. For non-competitive assays, 10^6 whole bone marrow cells
545 from a donor control (*RpS12*$^{flox/flox}$ or *RpS12*$^{flox/+}$) or *RpS12*$^{KO/+}$ mouse (CD45.2) were
546 injected into the retro-orbital venous sinus of recipient mice under isoflurane anesthesia.
547 For competitive transplants, 10^5 whole bone marrow cells from control *RpS12*$^{flox/+}$ or
548 *RpS12*$^{KO/+}$ donor mouse (CD45.2), and 10^5 competitor cells from a B6.SJL (CD45.1)
549 mouse were injected into each recipient mouse. Mice were given drinking water treated
550 with 100mg/ml Baytril100 (Bayer) for 3 weeks after transplantation. Peripheral blood was

551 collected every 4 weeks and animals were euthanized at the specified experimental time
552 points.
553
554 **Western blot analysis**
555 Whole bone marrow cells were enriched for cKit+ cells using CD117 MicroBeads and
556 MACS LS Columns (Miltenyi Biotec 130-091-224 and 130-042-401) following the
557 manufacturer's protocol. 2 x 10^6 cKit enriched cells were resuspended in 150 µl Laemmli
558 buffer (BioRad 1610737) supplemented with 1:10 β-mercaptoethanol, passed through a
559 25-G needle to break the DNA and incubated at 95°C for 5 minutes. An equal amount of
560 each sample was separated in polyacrylamide gels (BioRad 4568081), transferred to
561 nitrocellulose membrane (Licor) and blocked (Licor 927-90001). IRDye near-infrared
562 secondary antibodies (Licor) were used to visualize the proteins. The following primary
563 antibodies were used: RpS12 (Proteintech; polyclonal), β-actin (Cell Signaling; 13E5),
564 eIF2α (Cell signaling, 5324T), phospho-eIF2α (Thermo Scientific; Ser52; polyclonal).
565
566 **Histology**
567 Peripheral blood smears and cytospins from RBC lysed bone marrow samples were
568 stained using the Hema 3 System (Fisher) following the manufacturer's instructions. The
569 images were acquired using a Zeiss Axiovert microscope with a digital camera.
570
571 **Statistical methods**
572 Two-tailed Student's t-tests were performed to compare statistical significance between
573 two samples. When comparing more than 2 groups, one-way ANOVA tests were

574 performed with the Turkey's multiple comparison test. For presence/absence of
575 phenotype, statistical significance was calculated with Fisher's exact test. Analysis was
576 done using GraphPad Prism v9.

577

578 **Reagents**

579 All antibodies used for flow cytometry assays, and primers used for CRISPR gene editing
580 and PCR can be found in Supplementary Tables 1, 2, and 3. All other reagents are
581 mentioned in the methods section.

582

583 **Acknowledgments**

584 This work was supported by National Institutes of Health grants R01GM104213 (to
585 N.E.B.), R01CA196973 (to K.G.), an award from the Albert Einstein College of Medicine
586 Human Genetics Program (to N.E.B.), startup funds from the Albert Einstein College of
587 Medicine and Albert Einstein Cancer Center (to K.G.), the NHLBI/NIH Ruth L. Kirschstein
588 National Research Service Award F32HL146119 (to K.A.), and the IRACDA/BETTR
589 training Institutional Research and Academic Career Development Award
590 2K12GH102779-07A1 (to K.A). For flow cytometry this work utilized the analyzers Cytek
591 Aurora Multiparameter Flow Cytometer and BD LSR-II with the help from Dr. Jinghang
592 Zhang, Dr. Yu Zhang and Aodengtuya Fnu. The Cytek Aurora Multiparameter Flow
593 Cytometer was purchased with funding from the National Institutes of Health SIG grant
594 #1S10OD026833-01. Data in this paper are from a thesis to be submitted in partial
595 fulfillment of the requirements for the Degree of Doctor of Philosophy in the Biomedical
596 Sciences, Albert Einstein College of Medicine.

597

598

599 K.G. receives research funding from iOnctura, S.A. The authors have no additional
600 financial interests.

References

Baker NE. 2020. Emerging mechanisms of cell competition. *Nat Rev Genet* **21**: 683-697.

Boulan L, Andersen D, Colombani J, Boone E, Leopold P. 2019. Inter-Organ Growth Coordination Is Mediated by the Xrp1-Dilp8 Axis in Drosophila. *Dev Cell* **49**: 811-818 e814.

Brumwell A, Fell L, Obress L, Uniacke J. 2020. Hypoxia influences polysome distribution of human ribosomal protein S12 and alternative splicing of ribosomal protein mRNAs. *Rna* **26**: 361-371.

Cabezas-Wallscheid N, Buettner F, Sommerkamp P, Klimmeck D, Ladel L, Thalheimer FB, Pastor-Flores D, Roma LP, Renders S, Zeisberger P et al. 2017. Vitamin A-Retinoic Acid Signaling Regulates Hematopoietic Stem Cell Dormancy. *Cell* **169**: 807-+.

Chen C, Liu Y, Liu R, Ikenoue T, Guan KL, Liu Y, Zheng P. 2008. TSC-mTOR maintains quiescence and function of hematopoietic stem cells by repressing mitochondrial biogenesis and reactive oxygen species. *J Exp Med* **205**: 2397-2408.

Clavería C, Torres M. 2016. Cell Competition: Mechanisms and Physiological Roles. *Annual Review of Cell and Developmental Biology* **32**: 411-439.

de la Cruz J, Karbstein K, Woolford JL, Jr. 2015. Functions of ribosomal proteins in assembly of eukaryotic ribosomes in vivo. *Annu Rev Biochem* **84**: 93-129.

Derenzini E, Agostinelli C, Rossi A, Rossi M, Scellato F, Melle F, Motta G, Fabbri M, Diop F, Kodipad AA et al. 2019. Genomic alterations of ribosomal protein genes in diffuse large B cell lymphoma. *Br J Haematol* **185**: 330-334.

Fonseca BD, Smith EM, Yelle N, Alain T, Bushell M, Pause A. 2014. The ever-evolving role of mTOR in translation. *Seminars in cell & developmental biology* **36**: 102-112.

Galvez E, Vallespin E, Arias-Salgado EG, Sanchez-Valdepenas C, Gimenez Y, Navarro S, Rio P, Bogliolo M, Pujol R, Peiro M et al. 2021. Next-generation Sequencing in Bone Marrow Failure Syndromes and Isolated Cytopenias: Experience of the Spanish Network on Bone Marrow Failure Syndromes. *Hemasphere* **5**: e539.

Geiger T, Wehner A, Schaab C, Cox J, Mann M. 2012. Comparative proteomic analysis of eleven common cell lines reveals ubiquitous but varying expression of most proteins. *Mol Cell Proteomics* **11**: M111.014050-M014111.014050.

Gentilella A, Kozma SC, Thomas G. 2015. A liaison between mTOR signaling, ribosome biogenesis and cancer. *Biochimica et biophysica acta* **1849**: 812-820.

Ghemlas I, Li H, Zlateska B, Klaassen R, Fernandez CV, Yanofsky RA, Wu J, Pastore Y, Silva M, Lipton JH et al. 2015. Improving diagnostic precision, care and syndrome definitions using comprehensive next-generation sequencing for the inherited bone marrow failure syndromes. *J Med Genet* **52**: 575-584.

Hidalgo San Jose L, Sunshine MJ, Dillingham CH, Chua BA, Kruta M, Hong Y, Hatters DM, Signer RAJ. 2020. Modest Declines in Proteome Quality Impair Hematopoietic Stem Cell Self-Renewal. *Cell Rep* **30**: 69-80 e66.

Jaako P, Flygare J, Olsson K, Quere R, Ehinger M, Henson A, Ellis S, Schambach A, Baum C, Richter J et al. 2011. Mice with ribosomal protein S19 deficiency develop bone marrow failure and symptoms like patients with Diamond-Blackfan anemia. **118**: 6087-6096.

Ji Z, Kiparaki M, Folgado V, Kumar A, Blanco J, Rimesso G, Chuen J, Liu Y, Zheng D, Baker NE. 2019. Drosophila RpS12 controls translation, growth, and cell competition through Xrp1. *PLoS Genet* **15**: e1008513.

Kale A, Ji Z, Kiparaki M, Blanco J, Rimesso G, Flibotte S, Baker NE. 2018. Ribosomal Protein S12e Has a Distinct Function in Cell Competition. *Dev Cell* **44**: 42-55 e44.

Katanaev VL, Kryuchkov M, Averkov V, Savitsky M, Nikolaeva K, Klimova N, Khaustov S, Solis GP. 2020. HumanaFly: high-throughput transgenesis and expression of breast cancer transcripts in Drosophila eye discovers the RPS12-Wingless signaling axis. *Sci Rep* **10**: 21013.

Kazerounian S, Ciarlini PDSC, Yuan D, Ghazvinian R, Alberich-Jorda M, Joshi M, Zhang H, Beggs AH, Gazda HT. 2016. Development of Soft Tissue Sarcomas in Ribosomal Proteins L5 and S24 Heterozygous Mice. *Journal of Cancer* **7**: 32-36.

Kharas MG, Okabe R, Ganis JJ, Gozo M, Khandan T, Paktinat M, Gilliland DG, Gritsman K. 2010. Constitutively active AKT depletes hematopoietic stem cells and induces leukemia in mice. *Blood* **115**: 1406-1415.

Kondrashov N, Pusic A, Stumpf CR, Shimizu K, Andrew, Xue S, Ishijima J, Shiroishi T, Barna M. 2011. Ribosome-Mediated Specificity in Hox mRNA Translation and Vertebrate Tissue Patterning. *Cell* **145**: 383-397.

Krieg J, Hofsteenge J, Thomas G. 1988. Identification of the 40 S ribosomal protein S6 phosphorylation sites induced by cycloheximide. *The Journal of biological chemistry* **263**: 11473-11477.

Lee JY, Nakada D, Yilmaz OH, Tothova Z, Joseph NM, Lim MS, Gilliland DG, Morrison SJ. 2010. mTOR activation induces tumor suppressors that inhibit leukemogenesis and deplete hematopoietic stem cells after Pten deletion. *Cell stem cell* **7**: 593-605.

Magee JA, Ikenoue T, Nakada D, Lee JY, Guan KL, Morrison SJ. 2012. Temporal Changes in PTEN and mTORC2 Regulation of Hematopoietic Stem Cell Self-Renewal and Leukemia Suppression. *Cell stem cell* **11**: 415-428.

Magee JA, Signer RAJ. 2021. Developmental Stage-Specific Changes in Protein Synthesis Differentially Sensitize Hematopoietic Stem Cells and Erythroid Progenitors to Impaired Ribosome Biogenesis. *Stem Cell Reports* **16**: 20-28.

Martin-Villanueva S, Fernandez-Fernandez J, Rodriguez-Galan O, Fernandez-Boraita J, Villalobo E, de La Cruz J. 2020. Role of the 40S beak ribosomal protein eS12 in ribosome biogenesis and function in Saccharomyces cerevisiae. *RNA Biol* **17**: 1261-1276.

Marygold SJ, Roote J, Reuter G, Lambertsson A, Ashburner M, Millburn GH, Harrison PM, Yu Z, Kenmochi N, Kaufman TC et al. 2007. The ribosomal protein genes and Minute loci of Drosophila melanogaster. *Genome Biol* **8**: R216.

Matsson H, Davey EJ, Draptchinskaia N, Hamaguchi I, Ooka A, Leveen P, Forsberg E, Karlsson S, Dahl N. 2004. Targeted Disruption of the Ribosomal Protein S19 Gene Is Lethal Prior to Implantation. **24**: 4032-4037.

McGowan KA, Li JZ, Park CY, Beaudry V, Tabor HK, Sabnis AJ, Zhang W, Fuchs H, De Angelis MH, Myers RM et al. 2008. Ribosomal mutations cause p53-mediated dark skin and pleiotropic effects. *Nature Genetics* **40**: 963-970.

Morata G, Ripoll P. 1975. Minutes: Mutants of Drosophila autonomously affecting cell division rate. *Developmental Biology* **42**: 211-221.

Morgado-Palacin L, Varetti G, Llanos S, Gomez-Lopez G, Martinez D, Serrano M. 2015. Partial Loss of Rpl11 in Adult Mice Recapitulates Diamond-Blackfan Anemia and Promotes Lymphomagenesis. *Cell Rep* **13**: 712-722.

Muramatsu H, Okuno Y, Yoshida K, Shiraishi Y, Doisaki S, Narita A, Sakaguchi H, Kawashima N, Wang X, Xu Y et al. 2017. Clinical utility of next-generation sequencing for inherited bone marrow failure syndromes. *Genet Med* **19**: 796-802.

Oliver ER, Saunders TL, Tarle SA, Glaser T. 2004. Ribosomal protein L24 defect in belly spot and tail (Bst), a mouse Minute. *Development* **131**: 3907-3920.

692 Petibon C, Malik Ghulam M, Catala M, Abou Elela S. 2020. Regulation of ribosomal protein genes: An
693 ordered anarchy. *Wiley Interdiscip Rev RNA*: e1632.
694 Pietras EM, Reynaud D, Kang YA, Carlin D, Calero-Nieto FJ, Leavitt AD, Stuart JM, Gottgens B, Passegue E.
695 2015. Functionally Distinct Subsets of Lineage-Biased Multipotent Progenitors Control Blood
696 Production in Normal and Regenerative Conditions. *Cell Stem Cell* **17**: 35-46.
697 Roux PP, Shahbazian D, Vu H, Holz MK, Cohen MS, Taunton J, Sonenberg N, Blenis J. 2007. RAS/ERK
698 signaling promotes site-specific ribosomal protein S6 phosphorylation via RSK and stimulates cap-
699 dependent translation. *J Biol Chem* **282**: 14056-14064.
700 Roux PP, Topisirovic I. 2018. Signaling Pathways Involved in the Regulation of mRNA Translation. *Mol Cell*
701 *Biol* **38**.
702 Schalm SS, Fingar DC, Sabatini DM, Blenis J. 2003. TOS motif-mediated raptor binding regulates 4E-BP1
703 multisite phosphorylation and function. *Current biology : CB* **13**: 797-806.
704 Schneider RK, Schenone M, Ferreira MV, Kramann R, Joyce CE, Hartigan C, Beier F, Brummendorf TH,
705 Germing U, Platzbecker U et al. 2016. Rps14 haploinsufficiency causes a block in erythroid
706 differentiation mediated by S100A8 and S100A9. *Nat Med* **22**: 288-297.
707 Signer RA, Magee JA, Salic A, Morrison SJ. 2014. Haematopoietic stem cells require a highly regulated
708 protein synthesis rate. *Nature* **509**: 49-54.
709 Sigurdsson V, Miharada K. 2018. Regulation of unfolded protein response in hematopoietic stem cells. *Int*
710 *J Hematol* **107**: 627-633.
711 Socolovsky M, Nam H-S, Fleming MD, Haase VH, Brugnara C, Lodish HF. 2001. Ineffective erythropoiesis
712 in Stat5a−/−5b−/− mice due to decreased survival of early erythroblasts. *Blood* **98**: 3261-3273.
713 Sugiyama D, Inoue-Yokoo T, Fraser ST, Kulkeaw K, Mizuochi C, Horio Y. 2011. Embryonic regulation of the
714 mouse hematopoietic niche. *ScientificWorldJournal* **11**: 1770-1780.
715 Terzian T, Dumble M, Arbab F, Thaller C, Donehower LA, Lozano G, Justice MJ, Roop DR, Box NF. 2011.
716 Rpl27a mutation in the sooty foot ataxia mouse phenocopies high p53 mouse models. *The Journal*
717 *of Pathology* **224**: 540-552.
718 Ulirsch JC, Verboon JM, Kazerounian S, Guo MH, Yuan D, Ludwig LS, Handsaker RE, Abdulhay NJ, Fiorini C,
719 Genovese G et al. 2018. The Genetic Landscape of Diamond-Blackfan Anemia. *Am J Hum Genet*
720 **103**: 930-947.
721 Watkins-Chow DE, Cooke J, Pidsley R, Edwards A, Slotkin R, Leeds KE, Mullen R, Baxter LL, Campbell TG,
722 Salzer MC et al. 2013. Mutation of the diamond-blackfan anemia gene Rps7 in mouse results in
723 morphological and neuroanatomical phenotypes. *PLoS Genet* **9**: e1003094.
724 Wek RC, Jiang HY, Anthony TG. 2006. Coping with stress: eIF2 kinases and translational control. *Biochem*
725 *Soc Trans* **34**: 7-11.
726 Wilson DN, Doudna Cate JH. 2012. The structure and function of the eukaryotic ribosome. *Cold Spring*
727 *Harb Perspect Biol* **4**.
728 Yilmaz OH, Valdez R, Theisen BK, Guo W, Ferguson DO, Wu H, Morrison SJ. 2006. Pten dependence
729 distinguishes haematopoietic stem cells from leukaemia-initiating cells. *Nature* **441**: 475-482.
730 Yonath A, Franceschi F. 1998. Functional universality and evolutionary diversity: insights from the
731 structure of the ribosome. *Structure* **6**: 679-684.

732

Figure 4. Heterozygous loss of *RpS12* impairs HSCs ability to reconstitute peripheral blood.
(A) Non-competitive BM transplant strategy testing the long-term reconstituting activity of $RpS12^{KO/+}$ HSCs. 10^6 bone marrow cells from $RpS12^{KO/+}$ or $RpS12^{flox/flox}$ samples (CD45.2+) were transplanted into lethally irradiated B6.SJL (CD45.1+) mice, peripheral blood chimerism was determined every 4 weeks. **(B)** Kaplan-Meier survival curves of mice transplanted with BM cells from $RpS12^{KO/+}$ and control $RpS12^{flox/+}$ or $RpS12^{flox/flox}$ mice (control n=20 and KO/+ n=20 transplanted mice, combination of 2 independent non-competitive transplants with 1 donor per genotype transplanted into 10 host mice each). **(C)** Frequency of recipient mice with long-term (20-weeks) multi-lineage reconstitution (≥0.5% in all three macrophages, B, and T cells)(control n=20 and KO/+ n=20 transplanted mice, combination of 2 independent non-competitive transplants). **(D-G)** Peripheral blood donor derived **(D)** total chimerism and **(E-G)** multi-lineage chimerism in non-competitively transplanted whole bone marrow (CD45.2+) recipients (flox/flox n=10 and KO/+ n=10). **(H)** Schematic representation of the competitive bone marrow transplant. $5x10^5$ cells from $RpS12^{KO/+}$ or $RpS12^{flox/+}$ donor bone marrow (CD45.2+) mixed with $5x10^5$ competitor bone marrow cells from B6.SJL (CD45.1+) mice were injected into lethally irradiated B6.SJL (CD45.1+) mice. Chimerism in peripheral blood was determined every 4 weeks and bone marrow chimerism was analyzed at 20 weeks after transplant. **(I)** Total bone marrow chimerism and **(J)** HSCs donor-derived (CD45.2+) chimerism in the recipient bone marrow (Flox/+ n=10 and KO/+ n=10 competitive-transplanted mice). **(K-N)** Donor derived peripheral blood chimerism of competitively transplanted $RpS12^{KO/+}$ or $RpS12^{flox/+}$ bone marrow cells as described in **H**.
Non-competitive transplants were performed twice, using different controls: $RpS12^{flox/+}$ or $RpS12^{flox/flox}$. The competitive transplant was performed once, using $RpS12^{flox/+}$ mice as a control group
Statistical analysis: data represent mean +/-SEM, unpaired t-tests were performed to assess significance among populations between genotypes *p < 0.05, **p < 0.01 , ***p < 0.001, ****p < 0.0001

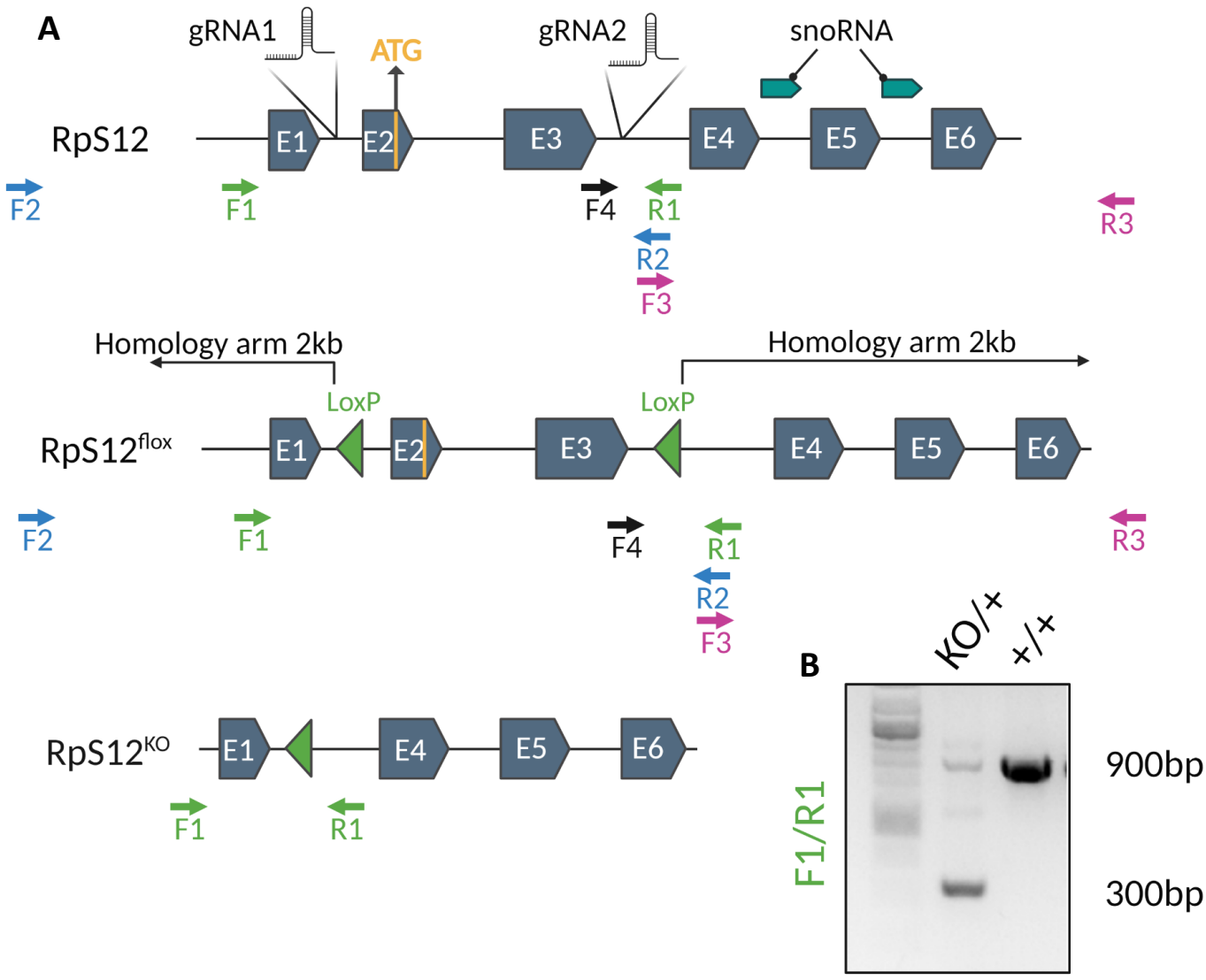

Supplementary Figure 1. CRISPR gene editing and genotyping strategy for the generation of *RpS12^{Flox}* and *RpS12^{KO}*

(A) Diagram of the WT, Flox and KO alleles of RpS12 generated in this study indicating the position of Snord100 and Snora33 (snoRNA),Cas9 gRNAs target locations, and primers used for genotyping. The homology arms starting sites are indicated and the ends fall outside of the RpS12 locus. To identify the first transformants, two pair of primers were used for PCR amplification: F2/R2 and F3/R3. F2 and R3 fall outside of the sequence covered by the homology arms, to ensure the inserts are on the correct location. The presence of LoxP sites was confirmed by Sanger sequencing using primers F1 and F4 for F2/R2 fragments, and with F3 and R3 for F3/R3 fragments. To determine excision of exon 2 and 3 by Cre recombination primers F1 and R1 were used, which generate a 900bp fragment in *RpS12*$^{+}$ and a 300bp fragment in *RpS12^{KO}* **(B)**.

Supplementary table 1

Oligo Name	Sequence
gRNA 1	CGCAGTAGACACGCTATCGCCGG
gRNA 2	GTGGGTTGCTGTGTGGATCGGGG
F1	GCACATGCGCACAGAAGT
R1	CGGACTATCTATCCCCACGA
F2	GTACAGCTATCTGCCAGGAA
R2	CGAGGTCGACGGTATCG
F3	CGATACCGTCGACCTCG
R3	GTGCTAGCAACAGAAGGTTC
F4	GTCTCAATACTGTGGGGTGT

Supplementary Table 2

		Antibodies	Clone	Source	Catalog Number
		Peripheral blood flow			
	Peripheral blood after Transplant	CD16/CD32	Clone 2.4G2	BD biosciences	553142
		Gr1 APC Cy7	RB6-8C5	BD biosciences	557661
		Mac1 PE	M1/70	BioLegend	101208
		B220 A700	RA3-6B2	BD biosciences	557957
		Thy1.2 APC	53-2.1	BD biosciences	553007
		CD45.1 FITC	A20	BD Biosciences	553775
		CD45.2 PE/Dazzle	104	BioLegend	109845
		Bone marrow flow on live cells			
Bone marrow after Transplant	Biotinylated lineage coctail	CD3e	145-2C11	eBioscience	13003182
		CD4	GK1.5	eBioscience	13004182
		CD8a	53-6.7	eBioscience	13008182
		Gr.1	RB68C5	eBioscience	13593182
		B220	RA3-6B2	eBioscience	13045282
		CD19	MB 19-1	eBioscience	13019182
		Ter119	TER119	eBioscience	13592182
	Conjugated	Sca1 PE-Cy7	D7	BioLegend	108114
		cKit APC	2B8	BD Biosciences	553356
		FCRg PE	93	Thermofisher	12-0161-81
		CD34e eF450	RAM34	Thermofisher	48-0341-80
		CD150 BV421	Q38-480	BD Biosciences	562811
		CD48 Alx700	HM48-1	BD Biosciences	560731
		Flk2-PE-Cy5	A2F10	BioLegend	135312
		CD45.2 *BV605*	104	BioLegend	109841
		CD45.1 FITC	A20	BD Biosciences	553775
		IL7R PerCP Cy5.5	SB/199	BD Biosciences	560733
		Streptavidin-APC-Cy7		BD Biosciences	554063
		Bone marrow flow on fixed cells			
Before fixation	Biotinylated lineage coctail	CD3e	145-2C11	eBioscience	13003182
		CD4	GK1.5	eBioscience	13004182
		CD8a	53-6.7	eBioscience	13008182
		Gr.1	RB68C5	eBioscience	13593182
		B220	RA3-6B2	eBioscience	13045282
		CD19	MB 19-1	eBioscience	13019182
		Ter119	TER-119	eBioscience	13592182
	Conjugated	Sca1 PE-Cy7	D7	eBioscience	25598182
		cKit APC	2B8	BD Biosciences	553356
		CD150 BV421	Q38-480	BD Biosciences	562811
		CD48 Alx700	HM48-1	BD Biosciences	560731
		Flk2-PE	A2F10	BioLegend	135310
		IL7R PerCP-Cy5	A7R34	BioLegend	135021
		Streptavidin-APC-Cy7		BD Biosciences	554063
Post fixation	Apoptosis	Annexin V		BD Biosciences	560931
		PI		BD Biosciences	556463
	p-Flow	pS6 (Ser235/236) Alexa 488	D57.2.2E	Cell Signaling	4803S
		pERK1(T202/Y204) Alexa 488	E10	Cell Signaling	4374
		pAkt (Ser473) AF647	193H12	Cell Signaling	2337
		p4E-BP1 (Thr37/46) AF647	236B4	Cell Signaling	5123
	Cell cycle	Ki-67 FITC	B56	BD Biosciences	556026
		Hoechst		BD Biosciences	

Supplementary Table 3

		Antibodies	Clone	Source	Catalog Number
		Bone marrow flow OPP			
Before fixation	Biotinylated lineage coctail	CD3e	145-2C11	eBioscience	13003182
		CD4	GK1.5	eBioscience	13004182
		CD8a	53-6.7	eBioscience	13008182
		Gr.1	RB68C5	eBioscience	13593182
		B220	RA3-6B2	eBioscience	13045282
		CD19	MB 19-1	eBioscience	13019182
		Ter119	TER-119	eBioscience	13592182
		IL7R	eBioRDR5	eBioscience	13127882
	Conjugated	Sca1 PE-Cy7	D7	eBioscience	25598182
		cKit APC	2B8	BD Biosciences	553356
		FCRg PE	93	Thermofisher	12-0161-81
		CD34e eF450	RAM34	Thermofisher	48-0341-80
		CD150 BV421	Q38-480	BD Biosciences	562811
		CD48 Alx700	HM48-1	BD Biosciences	560731
		Flk2-PE Cy5	A2F10	BioLegend	135311
		IL7R PerCP-Cy5	A7R34	BioLegend	135021
		Streptavidin-APC-Cy7		BD Biosciences	554063
	Non Conjugated	OPP		Thermofisher	C10456
After		Click-IT 488		Thermofisher	C10456
		Bone marrow and spleen (non-lysed)			
		CD16/CD32	Clone 2.4G2	BD biosciences	553142
		Ter119 APC	TER119	BioLegend	116211
		CD71 PE	C2	BD biosciences	561937